Inorg. Chem. **2008**, *47*, 11783−11797

Characterizations of Chloro and Aqua Mn(II) Mononuclear Complexes with Amino-Pyridine Ligands. Comparison of Their Electrochemical Properties With Those of Fe(II) Counterparts

Sihem Groni,[†] Christelle Hureau,*[,†,‡] Régis Guillot,[§] Geneviève Blondin,[†,||] Guillaume Blain,[§] and Elodie Anxolabéhère-Mallart*[,†]

Equipe de Chimie Inorganique, Institut de Chimie Moléculaire et des Matériaux d'Orsay, and Institut de Chimie Moléculaire et des Matériaux d'Orsay, Université Paris-Sud 11, UMR 8182 CNRS, Orsay F-91405, France

Received August 9, 2008

The solution behavior of mononuclear Mn(II) complexes, namely, $[(L_5^2)MnCl]^+$ (**1**), $[(L_5^3)MnCl]^+$ (**2**), $[(L_5^2)Mn(OH_2)]^{2+}$ (**3**), $[(L_5^3)Mn(OH_2)]^{2+}$ (**4**), and $[(L_6^2)Mn(OH_2)]^{2+}$ (**6**), with $L_5^{2/3}$ and L_6^2 being penta- and hexadentate amino-pyridine ligands, is investigated in MeCN using EPR, UV−vis spectroscopies, and electrochemistry. The addition of one chloride ion onto species **6** leads to the formation of the complex $[(L_6^2)MnCl]^+$ (**5**) that is X-ray characterized. EPR and UV−vis spectra indicate that structure and redox states of complexes **1**−**6** are maintained in MeCN solution. Chloro complexes **1**, **2**, and **5** show reversible Mn(II)/Mn(III) process at 0.95, 1.02, and 1.05 V vs SCE, respectively, whereas solvated complexes **3**, **4**, and **6** show an irreversible anodic peak around 1.5 V vs SCE. Electrochemical oxidations of **1** and **5** leading to the Mn(III) complexes $[(L_5^2)MnCl]^{2+}$ (**7**) and $[(L_6^2)MnCl]^{2+}$ (**8**) are successful. The UV−vis signatures of **7** and **8** show features associated with chloro to Mn(III) LMCT and d-d transitions. The X-ray characterization of the heptacoordinated Mn(III) species **8** is also reported. The analogous electrochemical generation of the corresponding Mn(III) complex was not possible when starting from **2**. The new mixed-valence di-μ-oxo $[(L_5^2)Mn(\mu O)_2Mn(L_5^2)]^{3+}$ species (**9**) can be obtained from **3**, whereas the sister $[(L_5^3)Mn(\mu O)_2Mn(L_5^3)]^{3+}$ species can not be generated from **4**. Such different responses upon oxidations are commented on with the help of comparison with related Mn/Fe complexes and are discussed in relation with the size of the metallacycle formed between the diamino bridge and the metal center (5- vs 6-membered). Lastly, a comparison between redox potentials of the studied Mn(II) complexes with those of Fe(II) analogues is drawn and completed with previously reported data on Mn/Fe isostructural systems. This gives us the opportunity to get some indirect insights into the metal specificity encountered in enzymes among which superoxide dismutase is the archetypal model.

Introduction

Manganese ions are involved in numerous crucial reactions performed by metalloenzymes and exist in different oxidation states in active sites of various nuclearities.[1,2] Binuclear sites are the most common and are found in catalase, ribonucleotide reductase, and arginase, whereas a tetranuclear Mn core is the heart of the oxygen evolving complex of photosystem II. A mononuclear Mn center is encountered in superoxide dismustase (SOD),[3,4] oxalate oxidase,[5,6] oxalate decarboxylase,[5,7] and lipoxygenase (LO).[8] Among the mononuclear Mn enzymes, the SOD that realizes disproportionation of superoxide ion into dioxygen and hydrogen peroxide[3,9] and the LO that catalyzes the dioxygenation of *cis*,*cis*-1,4-pentadiene containing fatty acids to alkyl hydroperoxides[10−12] have their Fe analogues.[10,13,14] Metal specificity depends on the host organism. FeLO are expressed in plant

* To whom correspondence should be addressed. E-mail: eanxolab@icmo.u-psud.fr (E.A.-M.); hureau@lcc-toulouse.fr (C.H.).
† Institut de Chimie Moléculaire et des Matériaux d'Orsay, Université Paris-Sud 11.
‡ Current Address: UPR 8241, Laboratoire de Chimie de Coordination, 205 Route de Narbonne, Toulouse Cedex 04, F-31077.
§ Institut de Chimie Moléculaire et des Matériaux d'Orsay, Université Paris-Sud 11.
|| Current Address: iRTSV/LCBM/PMB−UMR 5249 CNRS− CEA−UJF, 17 Rue des Martyrs, Grenoble Cedex 9, F-38054, France.

(1) Larson, E. J.; Pecoraro, V. L. Introduction to manganese enzymes. In *Manganese Redox Enzymes*; Pecoraro, V. L., Ed.; VCH Publishers: New York, 1992; pp 1−28.

10.1021/ic8015172 CCC: $40.75
Published on Web 11/13/2008

and animals, whereas the recently discovered MnLO is only found in fungi.[8] FeSOD are mainly found in bacteria, whereas MnSOD is located in mitochondria of animals but can also be inductively expressed in bacteria. With the exception of the so-called cambialistic,[15] MnSOD (FeSOD) are inactive when substituted with Fe (Mn). The metal active sites of Fe- and MnSOD has been proven to be structurally identical,[16] those of LO being proposed to be also very similar based on preliminary studies.[10,17,18] Taking into account the structural homology, the fact that these enzymes are involved in redox events and more precisely in proton coupled electron transfer (PCET) process may be anticipated as the origin of the metal dependent activity of the biological center.[19] In the case of SOD, an attractive hypothesis has been proposed by Miller et al. that relies on the 500 mV redox potentials differences for the MnSOD and Fe(Mn)SOD or FeSOD and Mn(Fe)SOD[20] determined for the noncambialistic *E.coli* SOD.[13] Moreover, the impact of the coordinated solvent molecules on the redox tuning of the active site has also been demonstrated.[21,22]

Bioinorganic chemists have paid attention to the functioning mode of such enzymes and hence to their structures and spectroscopic characterizations. Chemical preparation and electrochemical and spectroscopic investigations of bioinspired low-molecular-weight complexes is a way to gain structural and functional insights into the active sites of enzymes. With these objectives, we and others have investigated the design and characterizations of Mn mononuclear complexes. For example, very recent works consist in the study of water exchange rate constant on Mn(II) complexes bearing pentadentade ligands,[23] or in the synthesis of Mn(II) complexes with either pentadentate ligand based on a 1,2-ethanediamine moiety or tetradentate N-tripod ligands that exhibit strong SOD-like activity.[24−26] However, only some groups have explored the challenging task of unraveling the divergence between Mn vs Fe in bioinorganic models despite the high biological relevance of such studies. Examples include the characterization by Borovik et al.[27−29] of mononuclear Mn/Fe complexes with oxo and hydroxo exogenous ligands and their stabilization via hydrogen bonds with the ligand, such systems modeling the metal mediated H-atom abstraction, a fundamental process in biology. Stack's group have more specifically studied the C−H activation by mononuclear Mn/Fe hydroxide complexes with the aim to mimic the LO.[30,31] Lastly, Un et al. have very recently worked on the design of cambialistic synthetic models of SOD based on terpy ligand.[32]

In this context, we report here the electrochemical investigations of mononuclear Mn(II) complexes obtained with the penta- and hexadentate amino-pyridine ligands L_5^2, L_5^3, and L_6^2 (see Chart 1), in which the coordination spheres are completed with either a chloride ion or a water molecule: $[(L_5^2)MnCl](PF_6)$(**1**(PF_6)),$[(L_5^3)MnCl](PF_6)$(**2**(PF_6)),$[(L_5^2)Mn(OH_2)](BPh_4)_2$ (**3**$(BPh_4)_2$), $[(L_5^3)Mn(OH_2)](BPh_4)_2$ (**4**$(BPh_4)_2$), $[(L_6^2)MnCl](ClO_4)$ (**5**(ClO_4)), and $[(L_6^2)Mn(OH_2)](ClO_4)_2$ (**6**$(ClO_4)_2$). The X-ray structures of the four hexacoordinated Mn(II) complexes (**1**−**4**), as well as their solid-state characterization by HF-EPR spectroscopy and modeling by DFT calculations were recently reported in a companion paper.[33] The X-ray structure of the heptacoordinated complex $[(L_6^2)Mn(OH_2)](ClO_4)_2$ (**6**$(ClO_4)_2$) was described in a previous report,[34] and those of the corresponding chloro species in both the +II and +III oxidation states $[(L_6^2)MnCl](ClO_4)$ (**5**(ClO_4)) and $[(L_6^2)MnCl](ClO_4)_2$ (**8**$(ClO_4)_2$) are detailed

(2) Crowley, J. D.; Traynor, D. A.; Weatherburn, D. C. Enzymes and proteins containing manganese: an overview. In *Metals Ions in Biological Systems*; Sigel, A., Sigel, H., Eds.; Marcel-Dekker: Basel, Switzerland, 2000; Vol. *37*, pp 209−278.
(3) Whittaker, J. W. Manganese superoxide dismutases. In *Metal Ions in Biological Processes*; Sigel, A., Sigel, H., Eds.; Dekker Marcel: New York, 2000; Vol. *37*, pp 587−611.
(4) Fridovich, I. *Annu. Rev. Biochem.* **1995**, *64*, 97–112.
(5) Svedruzic, D.; Jonsson, S.; Toyota, C. G.; Reinhardt, L. A.; Ricagno, S.; Lindqvist, Y.; Richards, N. G. J. *Arch. Biochem. Biophys.* **2005**, *433*, 176–192.
(6) Opaleye, O.; Rose, R.-S.; Whittaker, M. M.; Woo, E.-J.; Whittaker, J. W.; Pickersgill, R. W. *J. Biol. Chem.* **2006**, *281*, 6428–6433.
(7) Just, V. J.; Stevenson, C. E. M.; Bowater, L.; Tanner, A.; Lawson, D. M.; Bornemann, S. *J. Biol. Chem.* **2004**, *279*, 19867–19874.
(8) Su, C.; Oliw, E. H. *J. Biol. Chem.* **1998**, *273*, 13072–13079.
(9) Whittaker, J. W. In *Superoxide Dismutase*; Packer, L., Ed.; Academic Press: New York, 2002; Vol. *37*, pp 80−90.
(10) Brash, A. R. *J. Biol. Chem.* **1999**, *274*, 23679–23682.
(11) Hamberg, M.; Su, C.; Oliw, E. *J. Biol. Chem.* **1998**, *273*, 13080–13088.
(12) Oliw, E. H.; Cristea, M.; Hamberg, M. *Lipids* **2004**, *39*, 319–323.
(13) Vance, C. K.; Miller, A.-F. *J. Am. Chem. Soc.* **1998**, *120*, 461–467.
(14) Maliekal, J.; Karapetian, A.; Vance, C.; Yikilmaz, E.; Wu, Q.; Jackson, T.; Brunold, T. C.; Spiro, T. G.; Miller, A.-F. *J. Am. Chem. Soc.* **2002**, *124*, 15064–15075.
(15) A small group of Mn/FeSOD, termed cambialistic superoxide dismutases, are active with either manganese or iron incorporated into the same active site.
(16) Lah, M. S.; Dixon, M. M.; Pattridge, K. A.; Stallings, W. C.; Fee, J. A.; Ludwig, M. L. *Biochemistry* **1995**, *34*, 1646–1660.
(17) Hörsten, L.; Su, C.; Osbourn, A. E.; Hellman, U.; Oliw, E. H *Eur. J. Biochem.* **2002**, *269*, 2690–2697.
(18) Cristea, M.; EngströmÅ.; Su, C.; Hörnsten, L.; Oliw, E. H *Arch. Biochem. Biophys.* **2005**, *434*, 201–211.
(19) Yikilmaz, E.; Porta, J.; Grove, L. E.; Vahedi-Faridi, A.; Bronshteyn, Y.; Brunold, T. C.; Borgstahl, G. E. O.; Miller, A.-F. *J. Am. Chem. Soc.* **2007**, *129*, 9927–9940.
(20) Fe(Mn)SOD (Mn(Fe)SOD) stands for the Fe substituted into the MnSOD protein (Mn substituted into the FeSOD protein).
(21) Miller, A.-F. *Acc. Chem. Res.* **2008**, *41*, 501–510.
(22) Grove, L. E.; Xie, J.; Yikilmaz, E.; Miller, A.-F.; Brunold, T. C. *Inorg. Chem.* **2008**, *47*, 3978–3992.
(23) Dees, A.; Zahl, A.; Puchta, R.; van Eikema Hommes, N. J. R.; Heinemann, F. W.; Ivanovic-Burmazovic, I. *Inorg. Chem.* **2007**, *46*, 2459–2470.
(24) Cisnetti, F.; Lefèvre, A.-S.; Guillot, R.; Lambert, F.; Blain, G.; Anxolabéhère-Mallart, E.; Policar, C. *Eur. J. Inorg. Chem.* **2007**, 4472–4480.
(25) Durot, S.; Lambert, F.; Renault, J.-P.; Policar, C. *Eur. J. Inorg. Chem.* **2005**, 2789–2793.
(26) Durot, S.; Policar, C.; Cisnetti, F.; Lambert, F.; Renault, J.-P.; Pelosi, G.; Blain, G.; Korri-Youssoufi, H.; Mahy, J.-P. *Eur. J. Inorg. Chem.* **2005**, 3513–3523.
(27) Borovik, A. S. *Acc. Chem. Res.* **2005**, *38*, 54–61.
(28) Gupta, R.; Borovik, A. S. *J. Am. Chem. Soc.* **2003**, *125*, 13234–13242.
(29) MacBeth, C. E.; Gupta, R.; Mitchell-Koch, K. R.; Young, V. G., Jr.; Lushington, G. H.; Thompson, W. H.; Hendrich, M. P.; Borovik, A. S. *J. Am. Chem. Soc.* **2004**, *126*, 2556–2567.
(30) Goldsmith, C. R.; Cole, A. P.; Stack, T. D. P. *J. Am. Chem. Soc.* **2005**, *127*, 9904–9912.
(31) Goldsmith, C. R.; Stack, T. D. P. *Inorg. Chem.* **2006**, *45*, 6048–6055.
(32) Sjödin, M.; Gätjens, J.; Tabares, L. C.; Thuéry, P.; Pecoraro, V. L.; Un, S. *Inorg. Chem.* **2008**, *47*, 2897–2908.
(33) Hureau, C.; Groni, S.; Guillot, R.; Blondin, G.; Duboc, C.; Anxolabéhère-Mallart, E. *Inorg. Chem.* **2008**, *47*, 9238–9247.
(34) Hureau, C.; Blanchard, S.; Nierlich, M.; Blain, G.; Rivière, E.; Girerd, J.-J.; Anxolabéhère-Mallart, E.; Blondin, G. *Inorg. Chem.* **2004**, *43*, 4415–4426.

Chart 1. Polydentate Amino-Pyridine Ligands Obtained from the Linear L_4^n Ligand, Built on the 1,2 Diamino-ethane ($n = 2$) or on the 1,3-Diamino-propane spacer ($n = 3$)[a]

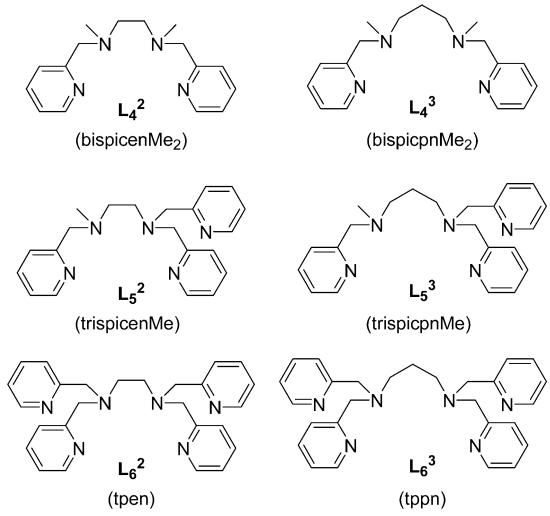

[a] Names based on usual nomenclature from literature are indicated in parentheses.

here as well as a new X-ray structure of complex $[(L_5^2)Mn(OH_2)](ClO_4)_2$ (**3′**$(ClO_4)_2$).

In the present work, we focus on acetonitrile (MeCN) solution studies of cations **1**−**6**. The data obtained are compared with those published in the literature of related Mn(II) complexes with tetradentate amino-pyridine ligands based on the linear L_4^n motif (see Chart 1) and with their Fe counterparts. This allows us to better characterize the individual chemical behavior of Mn/Fe complexes upon oxidation and to disentangle the influence of the size of the metallacycle with the diamino bridge (5- vs 6-membered) in the oxidation events. Last but not least, a more widespread comparison of redox properties of mononuclear Mn/Fe complexes is drawn with the objective to get deeper insights into the redox tuning of Mn vs Fe bioinspired chemical systems.

Experimental Section

General Remarks. Reagents and solvents were purchased commercially and used as received except for electrochemical experiments for which MeCN was distilled under argon over $CaCl_2$ granular. Argon U was used in the various experiments.

Caution. *Perchlorate salts of metal complexes with organic ligands are potentially explosive. Only small quantities of these compounds should be prepared and handled behind suitable protective shields.*

Syntheses. Syntheses of complexes $[(L_5^2)MnCl](PF_6)$ (**1**(PF_6)), $[(L_5^3)MnCl](PF_6)$ (**2**(PF_6)), $[(L_5^2)Mn(OH_2)](BPh_4)_2$ (**3**$(BPh_4)_2$), $[(L_5^3)Mn(OH_2)](BPh_4)_2$ (**4**$(BPh_4)_2$), and $[(L_6^2)Mn(OH_2)](ClO_4)_2$ (**6**$(ClO_4)_2$) have been described in previous papers,[33,34] in which the X-ray structures of the complexes have also been reported and detailed. The two new complexes $[(L_6^2)MnCl](ClO_4)$ (**5**(ClO_4)) and $[(L_6^2)MnCl](ClO_4)_2$ (**8**$(ClO_4)_2$) have been obtained in the present study by the addition of one equivalent of tetraethylammonium chloride (TEACl) on a MeCN solution of **6**, and by chemical oxidation of **5**, respectively.[35] Unfortunately, it was not possible to isolate them in sufficient amount for classical characterizations. However, for these two species, we were successful in obtaining crystals suitable for X-ray crystallography study.

X-ray Crystallography. Crystals of complexes $[(L_6^2)MnCl](ClO_4)$ (**5**(ClO_4)) were obtained by slow diffusion of diethyl ether in a MeCN solution of $[(L_6^2)Mn(OH_2)](ClO_4)_2$ (**6**$(ClO_4)_2$) in the presence of 1 equiv. of TEACl. Crystals of complexes $[(L_6^2)MnCl](ClO_4)_2$ (**8**$(ClO_4)_2$) were obtained by slow diffusion of diethyl ether in a MeCN solution of **5**(ClO_4) in the presence of 10 equiv. of TEACl and four equiv. of *meta*-chloro perbenzoic acid (*m*-CPBA). Crystals of complex $[(L_5^2)Mn(OH_2)](ClO_4)_2$ (**3′**$(ClO_4)_2$) were obtained from the evaporation of a MeCN solution containing L_5^2 and $[Mn(OH_2)_6](ClO_4)_2$ in a 1:1 stoichiometry, to which 1.5 equiv. of PhIO (methalonic solution) has been added. Crystal data for **5**$(ClO_4)\cdot CH_3CN$, **8**$(ClO_4)_2$, and **3′**$(ClO_4)_2$ were collected on a Bruker Kappa-X8 APEXII area detector diffractometer using graphite-monochromated Mo Kα radiation at ICMMO ORSAY, F-91405. Data were corrected for Lorentz-polarization. The structures were solved by the direct methods with SHELXS-97[36] and refined by full matrix least-squares on F^2 with anisotropic thermal parameters for all non H atoms with SHELXL-97.[37] H atoms were found in a difference Fourier map and were introduced at calculated positions as riding atoms, with C−H bond lengths of 0.93 (aromatic CH), 0.98 (aliphatic CH), 0.97 (CH_2), and 0.96 Å (CH_3), and with $U_{iso}(H)$ values of $1.2U_{eq}$(C) for CH and CH_2 H atoms, and $1.5U_{eq}$(C) for CH_3 H atoms. The drawing of the molecule was realized with the help of ORTEP32 for PC.[38] Details of structure determination, refinement and experimental parameters for compounds **5**$(ClO_4)\cdot CH_3CN$, **8**$(ClO_4)_2$, and **3′**$(ClO_4)_2$ are reported in Table 1. Crystallographic data for the structure reported in this paper have been deposited with the Cambridge Crystallographic Data Center, CCDC 684157, 684158, and 684159. Copies of this information may be obtained free of charge from The Director, CCDC, 12 Union Road, Cambridge, CB2 1EZ, U.K. (fax: 44-1223-336033; e-mail: deposit@ccdc.cam.ac.uk or http://www.ccdc.cam.ac.uk).

EPR Spectroscopy. 9.4 GHz EPR (X-band) spectra were recorded on a Bruker ELEXSYS 500 spectrometer. For low temperature studies, an Oxford Instrument continuous flow liquid helium cryostat and a temperature control system were used. Solutions spectra were routinely recorded in MeCN containing 0.1 or 0.2 M tetrabutylammonium perchlorate.

UV−visible Spectroscopy. UV−visible spectra were recorded on a Varian Cary 300 Bio spectrophotometer at 20 °C with 0.1 cm quartz cuvettes.

Cyclic Voltammetry and Bulk Electrolysis. All electrochemical experiments were run under an Ar atmosphere. Cyclic voltammetry and coulometry measurements were recorded on an EGG PAR potentiostat (M273 model). For cyclic voltammetry, the counter electrode was a Pt wire and the working electrode a glassy carbon disk carefully polished before each voltammogram with a 1 μm diamond paste, sonicated in ethanol bath and then washed carefully with ethanol. The reference electrode was a $Ag/AgClO_4$ electrode (0.3 V vs SCE), isolated from the rest of the solution by a fritted

(35) Despite several attempts, we were not able to obtain crystals of **8** from the electrolyzed solution of **5**. Consequently, we decided to obtain species **8** by chemical oxidation of species **6** by 4 equiv. of *m*-CPBA as the oxidant and in the presence of 10 equiv. of chloride ions.

(36) Sheldrick, G. M. *Program for Crystal Structure Solution, SHELXS-97*; University of Göttingen, Göttingen, Germany, 1997.

(37) Sheldrick, G. M. *Program for the Refinement of Crystal Structures from Diffraction Data, SHELXL-97*; University of Göttingen, Göttingen, Germany, 1997.

(38) Farrugia, L. J. *J. Appl. Crystallogr.* **1997**, *30*, 565.

Table 1. Details of Structure Determination, Refinement, and Experimental Parameters for Compounds $[(L_6^2)MnCl](ClO_4)$ (**5**$(ClO_4)\cdot CH_3CN$), $[(L_6^2)MnCl](ClO_4)_2$ (**8**$(ClO_4)_2$), and $[(L_5^2)Mn(OH_2)](ClO_4)_2$ (**3′**$(ClO_4)_2$)

	5$(ClO_4)\cdot CH_3CN$	**8**$(ClO_4)_2$	**3′**$(ClO_4)_2$
chemical formula	$(C_{26}H_{28}ClMnN_6)$, (C_2H_3N), (ClO_4)	$(C_{26}H_{28}ClMnN_6)$, $2(ClO_4)$	$(C_{21}H_{27}MnN_5O)$, $2(ClO_4)$
fw	655.44	713.83	619.32
cryst syst	monoclinic	monoclinic	orthorhombic
Space group	$P2_1/c$	$C2/c$	$Pna2_1$
a (Å)	14.4793(11)	15.069(5)	16.558(5)
b (Å)	10.1617(8)	10.094(5)	12.802(5)
c (Å)	20.4651(15)	19.429(5)	12.896(5)
α (deg)	90	90	90
β (deg)	92.0420(10)	94.530(5)	90
γ (deg)	90	90	90
V (Å^3)	3009.2(4)	2946.0(19)	2733.6(17)
Z	4	4	4
μ (Mo Kα) (mm^{-1})	0.663	0.780	0.735
cryst size (mm^3)	0.21 × 0.13 × 0.05	0.14 × 0.12 × 0.04	0.12 × 0.09 × 0.03
F(000)	1356	1464	1276
2θ range (deg)	2.66−30.16	2.43−27.51	2.92−26.99
T (K)	293(2)	293(2)	293(2)
no. of data collected	16 223	10 693	37 117
no. of unique data	7821	2851	5295
obsd data [$I > 2\sigma(I)$]	6216	2331	4484
R_{int} (%)	1.96	2.92	2.79
no. of params	380	201	351
R_1[a] (%)	5.44	6.91	7.21
wR_2[b] (%)	14.55	20.45	20.60
S [c]	1.046	1.067	1.055
$\Delta\rho_{min}$ (e$^-$ Å^{-3})	−0.843	−0.640	−0.577
$\Delta\rho_{max}$ (e$^-$ Å^{-3})	0.922	0.764	0.778

[a] $R_1 = \sum(|F_o| - |F_c|)/\sum|F_o|$. [b] $wR_2 = \{\sum[w(F_o^2 - F_c^2)^2]/\sum[w(F_o^2)^2]\}^{1/2}$ and $w = 1/[\sigma^2(F_o^2) + (aP)^2 + bP]$ with $P = [F_o^2 + 2F_c^2]/3$, $a = 0.1537$ (for 1) and 0.0353 (for 2), and $b = 0.8654$ (for 1) and 3.6214 (for 2). [c] Goodness of fit $= [\sum w(|F_o| - |F_c|)^2/(N_o - N_p)]^{1/2}$.

bridge. For bulk electrolysis, the counter electrode was a piece of Pt, separated from the rest of the solution with a fritted bridge. The working electrode was a grid of Pt. The solvent used was distilled MeCN and tetrabutylammonium perchlorate was added to obtain a 0.1 M supporting electrolyte (20 °C) or a 0.2 M supporting electrolyte (−30 °C). Low-temperature regulation was ensured by a Julabo circulation cryostat.

Results

We describe the solution behavior of four mononuclear Mn(II) complexes previously characterized in the solid state[33] and obtained with the amino-pyridine pentadentate ligands L_5^2 and L_5^3 (L_5^2 is the *N*-methyl-*N*,*N*′,*N*′-tris(2-pyridylmethyl)ethane-1,2-diamine and L_5^3 is the *N*-methyl-*N*,*N*′,*N*′-tris(2-pyridylmethyl)propane-1,3-diamine, see Chart 1), in which the coordination sphere are completed with either a chloride ion or a water molecule: $[(L_5^2)MnCl](PF_6)$ (**1**(PF_6)), $[(L_5^3)MnCl](PF_6)$ (**2**(PF_6)), $[(L_5^2)Mn(OH_2)](BPh_4)_2$ (**3**$(BPh_4)_2$), and $[(L_5^3)Mn(OH_2)](BPh_4)_2$ (**4**$(BPh_4)_2$)). We also report the X-ray crystal structure of species $[(L_5^2)Mn(OH_2)](ClO_4)_2$ (**3′**$(ClO_4)_2$), where **3** and **3′** show different configurations of the L_5^2 ligand. Lastly, we characterize the heptacoordinated Mn(II) and Mn(III) complexes obtained with the hexadentate amino-pyridine L_6^2 ligand (L_6^2 is the *N*,*N*,*N*′,*N*′-tetra(2-pyridylmethyl) ethane-1,2-diamine, see Chart 1) where the coordination sphere is completed with a chloride ion, $[(L_6^2)MnCl](ClO_4)$ (**5**(ClO_4)) and $[(L_6^2)MnCl](ClO_4)_2$ (**8**(ClO_4)), the characterization of the corresponding aqua species $[(L_6^2)Mn(OH_2)](ClO_4)_2$ (**6**$(ClO_4)_2$) being described in another paper.[34]

For purpose of clarity, we report in Table 2 the correspondence between the numbering of the complexes and their formula in MeCN solution, which are not rigorously identical to those determined from the X-ray structure. In particular, we have no way to distinguish between a MeCN or a water molecule as the coordinated solvent in the species issued from the dissolution in MeCN of **3**$(BPh_4)_2$ or **3′**$(ClO_4)_2$, **4**$(BPh_4)_2$), and **6**$(ClO_4)_2$. Label **5** refers to the $[(L_6^2)MnCl]^+$ cation in the solid state as well as the solution species resulting from the addition of 1 equiv. of chloride ion to a solution of **6**.

Table 2. Formula of Cations **1**−**10** in MeCN Solution

labeling	corresponding Mn(II) species in solution	labeling	corresponding Mn(III) and Mn(III)Mn(IV) species in solution
1	$[(L_5^2)MnCl]^+$	**7**	$[(L_5^2)MnCl]^{2+}$
2	$[(L_5^3)MnCl]^+$	**8**	$[(L_6^2)MnCl]^{2+}$
3	$[(L_5^2)Mn(solvent)]^{2+}$ [a]	**9**	$[(L_5^2)Mn(\mu O)_2Mn(L_5^2)]^{3+}$
4	$[(L_5^3)Mn(solvent)]^{2+}$ [a]	**10**	$[(L_6^2)Mn(\mu O)_2Mn(L_6^2)]^{3+}$
5	$[(L_6^2)Mn(solvent)]^{2+} + Cl^-$ [b]		
6	$[(L_6^2)Mn(solvent)]^{2+}$ [a]		

[a] Solvent = OH_2 or MeCN. Complexes obtained by dissolution of the corresponding water species in MeCN (**3**, **4**, and **6**) or in situ generated by the precipitation of the chloride ion from the corresponding chloro species (**1** and **2**) by addition of one equiv. of silver perchlorate. [b] Complex obtained by addition of one equivalent of chloride ion onto the corresponding species **6**.

X-ray Crystal Structures of Cations 3′, 5, and 8. Heptacoordinated complexes $[(L_6^2)MnCl]^+$ (5) and $[(L_6^2)MnCl]^{2+}$ (8). The ORTEP views of cations **5** and **8** are shown in Figure 1 and principal bond lengths and angles are listed in Table 3 with those of the previously described cation $[(L_6^2)Mn(OH_2)]^{2+}$ (**6**).[34] The common feature of complexes **5** and **8** are the heptacoordination obtained by the hexadentate L_6^2 ligand and the exogenous chloride ion. The molecular geometry around the Mn center can be described as a capped trigonal prism. The three nitrogen

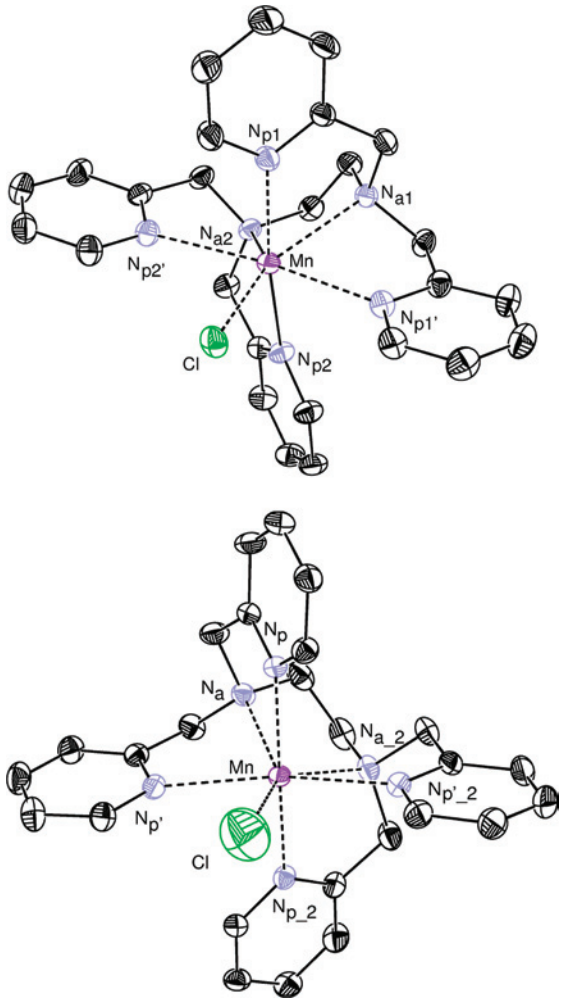

Figure 1. ORTEP drawings of the cations $[(L_6^2)MnCl]^+$ (**5**) (top) and $[(L_6^2)MnCl]^{2+}$ (**8**) (bottom) with the ellipsoids drawn at the 50% probability level. Atoms_2 were generated with the symmetry $-x, y, 1/2 - z$.

Table 3. Selected Bond Lengths (Å) and Angles (deg) for Cations $[(L_6^2)MnCl]^+$ (**5**), $[(L_6^2)Mn(OH_2)]^{2+}$ (**6**),[34] and $[(L_6^2)MnCl]^{2+}$ (**8**)

	5		**6** (from ref 34)	**8**
$Mn-N_{a1}$	2.444(2)	$Mn-N_a$	2.402(2)	2.392(4)
$Mn-N_{a2}$	2.485(2)	$Mn-N_p$	2.292(2)	2.293(3)
$Mn-N_{p1}$	2.262(2)	$Mn-N_{p'}$	2.463(2)	2.473(3)
$Mn-N_{p2}$	2.297(2)	Mn−X [a]	2.259(2)	2.273(5)
$Mn-N_{p1'}$	2.490(2)	$X-Mn-N_a$ [a]	142.82(5)	142.81(9)
$Mn-N_{p2'}$	2.498(2)	$X-Mn-N_p$ [a]	90.84(5)	91.00(9)
Mn−Cl	2.4544(7)	$X-Mn-N_{p'}$ [a]	80.87(5)	80.95(9)
$Cl-Mn-N_{a1}$	147.76(6)			
$Cl-Mn-N_{a2}$	139.44(6)			
$Cl-Mn-N_{p1}$	98.76(6)			
$Cl-Mn-N_{p2}$	90.80(6)			
$Cl-Mn-N_{p1'}$	83.24(6)			
$Cl-Mn-N_{p2'}$	83.74(6)			

[a] X = OH_2 in the case of **6** and X = Cl^- in the case of **8**.

atoms of one amine function and the two connected pyridine arms define the trigonal bases. The chloride ion caps the rectangular face defined by the four nitrogen atoms of the pyridine functions. The Mn−Cl bond coincides with a C_2 axis in **8**. The coordination spheres of the Mn centers are rather irregular due to the geometric constraints imposed by the ligand itself. In particular, two of the $Mn-N_{pyridine}$ bond distances are appreciably longer than the two others both in **5** (2.494(2) vs 2.279(2) Å, in average) and **8** (2.473(3) vs 2.293(3) Å). Significant difference in the bond distances between **5** and **8** are observed for the Mn−Cl (2.4544(7) vs 2.273(5) Å) and the $Mn-N_{amine}$ (2.464(2) in average vs 2.392(4) Å). These two shorter distances are observed in the Mn(III) complex **8**, whereas the $Mn-N_{pyridine}$ bond lengths are equivalent for the two oxidation states of the Mn center. This can thus be attributed to a compression along the C_2 axis due to Jahn−Teller effect upon oxidation of the Mn ion. Comparison of **5** with the corresponding aqua **6** evidences that the exogenous ligand is more distant from the Mn center in **5** than in **6**, an effect that is attributed to the greater bulkiness of the chloride ion compared to the one of the aqua molecule. Concomitantly, the $Mn-N_{amine}$ bonds are longer in the case of **5** due to the inductive trans effect of the chloride ion. Value of the Mn−Cl bond length in **5** lies in the range of [2.35−2.58 Å] obtained for $[N_5Cl]$ or $[N_5OCl]$ related complexes,[39−48] and is smaller than the one of 2.596 Å reported for a $[N_4O_2Cl]$ complex with a similar geometry.[41] The value of the Mn−Cl bond length in **8** lies in the low range limit of [2.218−2.476] determined for hexacoordinated Mn(III) with N,O ligands,[49−52] and is significantly shorter than the one of 2.52 Å reported for two $[N_4Cl_2]$ complexes.[53,54] This difference can be attributed to the trans position of two chloride ions in the latter species along the Cl−Mn−Cl Jahn−Teller elongation axis. The average values of the $Cl-Mn-N_{pyridine}$ angles are close to the theoretical value of 90° in **5**, whereas in **8**, this value is attained only when the pyridine nitrogen involved is the most distant from the Mn center. The $Cl-Mn-N_{amine}$ angles are close to 143° for both **5** and **8**.

Complex $[(L_5^2)Mn(OH_2)]^{2+}$ (3′). The ORTEP view of the cation **3′** (from $[(L_5^2)Mn(OH_2)](ClO_4)_2$) is compared in Figure 2 to the ORTEP view of the corresponding cation **3**

(39) Brudenell, S. J.; Spiccia, L.; Bond, A. M.; Fallon, G. D.; Hockless, D. C. R.; Lazarev, G.; Mahon, P. J.; Tiekink, E. R. T. *Inorg. Chem.* **2000**, *39*, 881–892.
(40) Collinson, S.; Alcock, N. W.; Raghunathan, A.; Kahol, P. K.; Busch, D. H. *Inorg. Chem.* **2000**, *39*, 757–764.
(41) El Ghachtouli, S.; Mohamadou, A.; Barbier, J.-P. *Inorg. Chim. Acta* **2005**, *358*, 3873–3880.
(42) Ghosh, K.; Eroy-Reveles, A. A.; Avila, B.; Holman, T. R.; Olmstead, M. M.; Mascharak, P. K. *Inorg. Chem.* **2004**, *43*, 2988–2997.
(43) Klein Gebbink, R. J. M.; Jonas, R. T.; Goldsmith, C. R.; Stack, T. D. P. *Inorg. Chem.* **2002**, *41*, 4633–4641.
(44) Lah, M. S.; Chun, H. *Inorg. Chem.* **1997**, *36*, 1782–1785.
(45) Li, Q.-X.; Luo, Q.-H.; Li, Y.-Z.; Pan, Z.-Q.; Shen, M.-C. *Eur. J. Inorg. Chem.* **2004**, 4445–4456.
(46) Wittmann, H.; Raab, V.; Schorm, A.; Plackmeyer, J.; Sundermeyer, J. *Eur. J. Inorg. Chem.* **2001**, 1937–1948.
(47) Tu, H.-Y.; Wang, C.-J.; Meng, X.-G.; Zhang, A.-D. *Acta Crystallogr., Sect. E* **2006**, *62*, m500–m501.
(48) Neumann, W. L.; Franklin, G. W.; Sample, K. R.; Aston, K. W.; Weiss, R. H.; Riley, D. P. *Tetrahedron Lett.* **1997**, *38*, 779–782.
(49) Sabater, L.; Hureau, C.; Guillot, R.; Aukauloo, A. *Inorg. Chem.* **2006**, *45*, 2373–2375.
(50) Triller, M. U.; Hsieh, W.-Y.; Pecoraro, V. L.; Rompel, A.; Krebs, B. *Inorg. Chem.* **2002**, *41*, 5544–5554.
(51) Triller, M. U.; Pursche, D.; Hsieh, W.-Y.; Pecoraro, V. L.; Rompel, A.; Krebs, B. *Inorg. Chem.* **2003**, *42*, 6274–6283.
(52) Reddig, N.; Pursche, D.; Rompel, A. *Dalton Trans.* **2004**, 1474–1480.
(53) Létumier, F.; Broeker, G.; Barbe, J.-M.; Guilard, R.; Lucas, D.; Dahaoui-Gindrey, V.; Lecomte, C.; Thouin, L.; Amatore, C. *J. Chem. Soc., Dalton Trans.* **1998**, 2233–2239.
(54) Shaikh, N.; Panja, A.; Banerjee, P.; Kubiak, M.; Ciunik, Z.; Puchalska, M.; Legendziewicz, J.; Vojtísek, P. *Inorg. Chim. Acta* **2004**, *357*, 25–32.

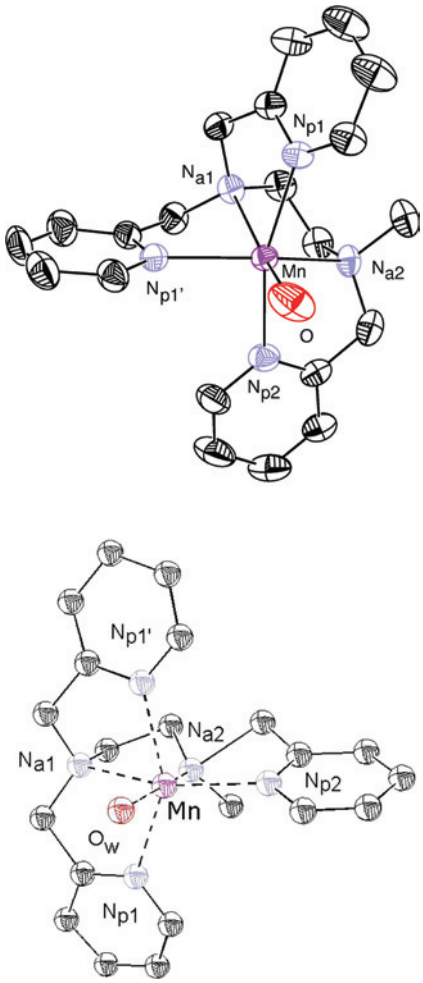

Figure 2. ORTEP drawings of the cations $[(L_5^2)Mn(OH_2)]^{2+}$ **3′** (top) and **3** (bottom) for comparison,[33] with the ellipsoids drawn at the 30% probability level.

(from $[(L_5^2)Mn(OH_2)](BPh_4)_2$). The L_5^2 ligand in **3** and **3′** adopt two different configurations, mer−trans in **3** and mer−cis in **3′**. The mer−cis and mer−trans configurations refer to a mer arrangement of the three pyridine groups, the two pyridine arms connected to the same amine function being either in cis or trans position, respectively (see Scheme 1). This difference may be related to the different counterions, ClO_4^- in case of **3′** and BPh_4^- in case of **3** (see Discussion Section). Principal bond lengths and angles of **3′** are listed in Table 4, where they are compared to those of **3**. The average values of the Mn−N_{amine} bond lengths are greater in **3′** (2.303(5) vs 2.224(17) Å) on the contrary to the average Mn−$N_{pyridine}$ and to the Mn−OH_2 bond lengths (2.253(6) vs 2.281(16) Å and 2.119(5) vs 2.212(15) Å, respectively). Bond lengths as well as angle values support geometry closer to the regular octahedron in **3**.

EPR Spectra of Complexes 1−6 in MeCN Solution. X-band EPR spectra recorded on frozen MeCN solution of Mn(II) complexes **1**−**6** are reproduced in Figure 3. They exhibit features from 0 to 0.8 T that can be interpreted as originating from a $S = 5/2$ electronic spin state with a zero-field-splitting (ZFS) effect in the 0.1 cm^{-1} order of magnitude.[34,55,56] Spectra of complexes $[(L_5^2)MnCl]^+$ (**1**) and $[(L_6^2)MnCl]^+$ (**5**) show well-resolved hyperfine lines. Six lines regularly spaced by 8 mT can be counted on the $g_{eff} = 9.3$ transition indicating the mononuclear character of **1** and **5** in solution ($I_{Mn} = 5/2$). The pattern of the $g_{eff} = 4.3$ transition is more complex due to the superimposition of several groups of hyperfine lines. Such 9.3 and 4.3 g_{eff} values are reminiscent of what is reported for isoelectronic high-spin Fe(III) complexes with a rhombic ZFS interaction.[57,58]

Scheme 1. Configurations of L_5 Ligand Encountered in the Present Study

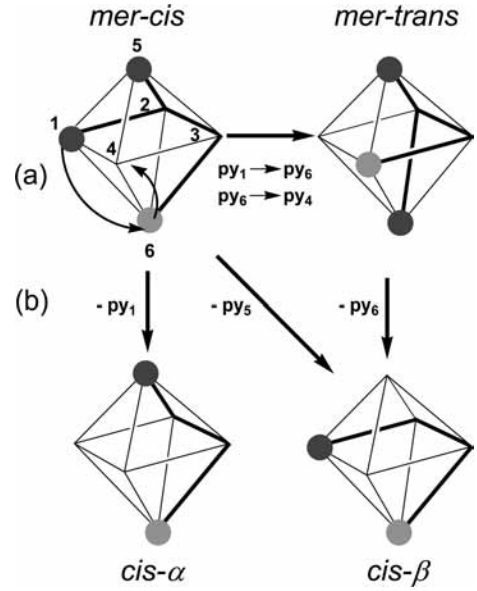

py_n corresponds to the pyridine function in position n, where the numbering of the positions is exemplified on the top left octahedron. The mer−cis (mer−trans) configuration corresponds to a mer arrangement of the three pyridine groups (gray circles), the two pyridine arms bound to the same amine function (dark gray circles) being in cis (trans) position. (a) Two-step interconversion of mer−cis leading to mer−trans configuration: the pyridine group in position 1 goes in position 6, whereas the one in position 6 goes in position 4. (b) One-step evolution of mer−cis and mer−trans to cis-α or cis-β configurations of the corresponding linear L_4 ligand: mer−cis to cis-α (cis-β) evolution is achieved by the decoordination of the pyridine group in position 1 (position 5), mer−trans to cis-β evolution is achieved by the decoordination of the pyridine group in position 6.

Table 4. Selected Bond Lengths (Å) and Angles (deg) for the Cations $[(L_5^2)Mn(OH_2)]^{2+}$ **3′** and **3**[33] (for comparison)

	3′	3 (from ref 33)
Mn−N_{a1}	2.294(5)	2.223(17)
Mn−N_{a2}	2.313(5)	2.226(15)
Mn−N_{p1}	2.252(5)	2.264(14)
Mn−N_{p2}	2.266(6)	2.265(16)
Mn−$N_{p1'}$	2.241(5)	2.314(13)
Mn-OH_2	2.119(5)	2.212(15)
OH_2−Mn−N_{a1}	162.8(3)	103.93(40)
OH_2−Mn−N_{a2}	111.6(3)	175.01(40)
OH_2−Mn−N_{p1}	91.7(2)	92.70(40)
OH_2−Mn−N_{p2}	89.9(3)	99.22(40)
OH_2−Mn−$N_{p1'}$	102.1(3)	87.54(30)

(55) Hureau, C.; Blondin, G.; Charlot, M.-F.; Philouze, C.; Nierlich, M.; Césario, M.; Anxolabéhère-Mallart, E. *Inorg. Chem.* **2005**, *44*, 3669–3683.
(56) Bucher, C.; Duval, E.; Barbe, J.-M.; Verpeaux, J.-N.; Amatore, C.; Guilard, R.; Le Pape, L.; Latour, J.-M.; Dahaoui, S.; Lecomte, C. *Inorg. Chem.* **2001**, *40*, 5722–5726.
(57) Peisach, J.; Blumberg, W. E.; Lode, E. T.; Coon, M. J. *J. Biol. Chem.* **1971**, *246*, 5877–5881.

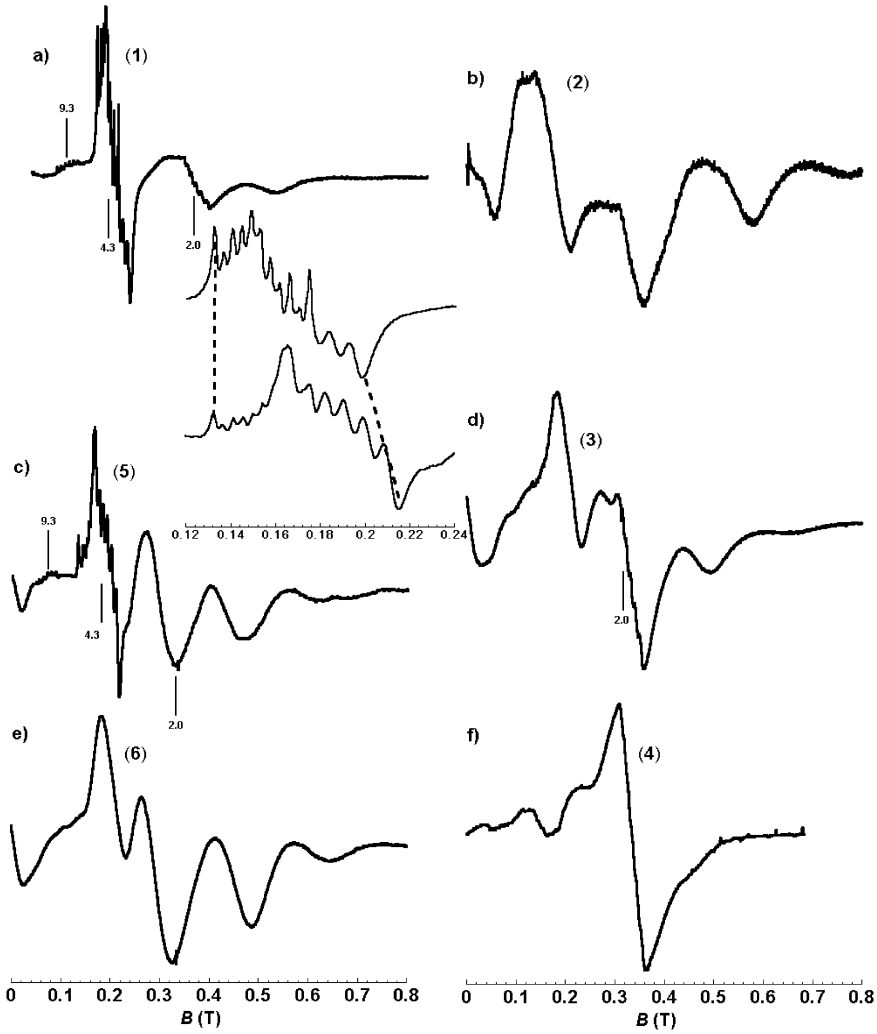

Figure 3. X-band EPR spectra of 2 mM MeCN solutions of (a) $[(L_5^2)MnCl]^+$ (**1**), (b) $[(L_5^3)MnCl]^+$ (**2**), (c) $[(L_6^2)MnCl]^+$ (**5**), (d) $[(L_5^2)Mn(solvent)]^{2+}$ (**3**), (e) $[(L_6^2)Mn(solvent)]^{2+}$ (**6**), and (f) $[(L_5^3)Mn(solvent)]^{2+}$ (**4**). Insets in (a) and (c): Zoom on the hyperfine pattern detected at $g_{eff} = 4.3$ for **1** (top) and **5** (bottom). Recording conditions (spectra a and b): 0.5 mT modulation amplitude, 0.123 mW microwave power, $T = 10$ K. Recording conditions (spectra c−f): 0.5 mT modulation amplitude, 2.0 mW microwave power, $T = 100$ K.[69]

Furthermore, as can be seen in the inset in Figure 3, the $g_{eff} = 4.3$ hyperfine pattern of **5** is slightly larger than the one of **1**, indicating that complexes **1** and **5** have different ZFS values. Hyperfine structures are lacking in the X-band signature of complexes $[(L_5^3)MnCl]^+$ (**2**), $[(L_5^2)Mn(solvent)]^{2+}$ (**3**),[59] $[(L_5^3)Mn(solvent)]^{2+}$ (**4**), and $[(L_6^2)Mn(solvent)]^{2+}$ (**6**). Such broadening of the hyperfine structure suggests that there is a structural or chemical heterogeneity in the sample. The structural heterogeneity is encountered when complexes do not exist with a well-defined coordination sphere in solution. This may be related to the greater flexibility of the L^3 vs L^2 ligands (**2** vs. **1** and **5**), as was already noticed in case of $[(L_4^2)MnCl_2]$ vs $[(L_4^3)MnCl(solvent)]^+$.[55] The chemical heterogeneity can be due to the lability of the water ligand that can be substituted by a MeCN solvent molecule (**3**, **4**, and **6**) and/or to the generation of different isomers upon dissolution (**2**, **3**, and **4**). In the particular case of **4**, the signal is reminiscent of what is observed for weakly coupled dinuclear Mn(II) systems,[60−65] suggesting that such dimeric species could be formed in solution. Hyperfine features are detected at $g_{eff} = 2$ in the spectra of complexes **1** and **3** that likely correspond to small amount (<5%) of uncoordinated Mn(II) species.[66] In that case, this $g_{eff} = 2$ signal indicates that the binding affinity of the Mn(II) ion is slightly diminished in case of

(58) Mabbs, F. E.; Collison, D., *Electron Paramagnetic Resonance of d Transition Metal Compounds*; Elsevier Science: Amsterdam, 1992; Vol. *16*.

(59) Note that the nature of the counter ion has no influence on the X-band EPR spectrum of a MeCN solution of $[(L_5^2)Mn(solvent)]^{2+}$ (see the Results dealing with cyclic voltammetry of **3** and **4**).

(60) Blanchard, S.; Blain, G.; Rivière, E.; Nierlich, M.; Blondin, G. *Chem.—Eur. J.* **2003**, *9*, 4260–4268.

(61) Blanchard, S.; Blondin, G.; Rivière, E.; Nierlich, M.; Girerd, J.-J. *Inorg. Chem.* **2003**, *42*, 4568–4578.

(62) Hureau, C.; Sabater, L.; Anxolabéhère-Mallart, E.; Nierlich, M.; Charlot, M.-F.; Gonnet, F.; Rivière, E.; Blondin, G. *Chem.—Eur. J.* **2004**, *10*, 1998–2010.

(63) Adams, H.; Bailey, N. A.; Debaecker, N.; Fenton, D. E.; Kanda, W.; Latour, J.-M.; Okawa, H.; Sakiyama, H. *Angew. Chem., Int. Ed.* **1995**, *34*, 2535–2537.

(64) Fernández, G.; Montserra, C.; Mahía, J.; Maestro, M. A. *Eur. J. Inorg. Chem.* **2002**, 2502–2510.

(65) Samples, C. R.; Howard, T.; Raushel, F. M.; DeRose, V. J. *Biochemistry* **2005**, *44*, 11005–11013.

(66) We can not exclude that the $g_{eff} = 2$ signal are part of the EPR spectra of complexes **1** and **3**.

L_5^2 ligands compared to that of L_5^3 and L_6^2. Lastly, the EPR signatures of **5** and **6** show similar strong transitions, hyperfine features being detected only in the spectrum of **5**. The almost identical EPR signatures of **5** and **6** indicate that complexes **5** and **6** have similar ZFS parameters. This may be due to a weak impact of the chloride ion on the ZFS parameters in **5**, an effect that can be related to the significantly long Mn—Cl bond length.[67,68] We have also considered that the similar EPR signatures of **5** and **6** may reveal an equilibrium between complexes **5** and **6**. However, we would then expect the two signatures to be superimposable which is not the case.

UV−Visible Spectra of Complexes 1−6 in MeCN Solution. The UV−vis spectra of complexes **1**−**6** do not show absorbance in the visible region, as expected for Mn(II) species. Spectra of the chloro complexes **1**, **2**, and **5**, recorded in MeCN show an intense band at 260 nm that is attributed to pyridine $\pi-\pi^*$ transitions of the ligand. The calculated ε extinction coefficient values are 7200 M^{-1} cm^{-1} for **1**, 8200 M^{-1} cm^{-1} for **2**, and 11700 M^{-1} cm^{-1} for **5**. The increase in the extinction coefficient value in comparison with the one reported for the parent complex $[(L_4^2)MnCl_2]$ ($\varepsilon = 4100$ M^{-1} cm^{-1})[55] is attributed to the additional pyridine group(s). Spectra of MeCN solution of the solvated complexes **3**, **4**, and **6** also show an intense band at 260 nm with ε values of 25 000 M^{-1} cm^{-1} for **3**, 16 000 M^{-1} cm^{-1} for **4**, and 19 200 M^{-1} cm^{-1} for **6**.

Electrochemical Studies of Complexes 1−6 in MeCN Solution. Chloro Complexes 1, 2, and 5. Solutions of complexes $[(L_5^2)MnCl](PF_6)$ (**1**(PF_6)) and $[(L_5^3)MnCl](PF_6)$ (**2**(PF_6)) as well as in situ generated species $[(L_6^2)MnCl]^+$ (**5**) (addition of one chloride ion on the solution of complex $[(L_6^2)Mn(OH_2)](ClO_4)_2$ (**6**$(ClO_4)_2$) were investigated by cyclic voltammetry at room temperature and 0 °C (**1**), −30 °C (**2**), and −20 °C (**5**) (Figure 4, solid lines). Cyclic voltammetry of **1** in MeCN solution at room temperature (Figure 4a) shows one quasi-reversible anodic wave (peaks 1 and 1′) at $E_{1/2} = 0.95$ V vs SCE ($\Delta E_p = 80$ mV, $i_1/i_{1'} \approx 1$) that can be attributed to the Mn(II)/Mn(III) oxidation process (see Table 5). The 1 e^-/Mn process is confirmed by preparative scale electrolysis (see below). We shall remark that the free chloride oxidation peak at 1.3 V vs SCE is not observed, thus indicating that in MeCN solution the chloride ion remains coordinated to the Mn center. A second anodic peak is observed at $E_p = 1.75$ V vs SCE (data not shown). At low temperature 0 °C (Figure 4b) this second anodic process become quasi-reversible and an anodic wave attributed to the formation of a Mn(IV) species (peaks 2 and 2′) is observed at $E_{1/2} = 1.65$ V vs SCE ($\Delta E_p = 125$ mV, $i_2/i_{2'} \approx 1$). The reactive Mn(IV) species is detected only if the temperature is lowered or the scan rate is increased (5 V s^{-1}). Room temperature cyclic voltammetry traces of **2** and **5** (panels c and e in Figure 4, respectively) show one quasi-reversible anodic process at $E_{1/2} = 1.02$ V vs SCE ($\Delta E_p = 85$ mV, $i_2/i_{2'} \approx 1$) (**2**) and $E_{1/2} = 1.05$ V vs SCE ($\Delta E_p = 93$ mV, $i_2/i_{2'} \approx 1$) (**5**), these values being 70 and 100 mV higher than the one observed for complex **1** (see Table 5). Unlike in complex **1**, the second anodic process detected for **2** at $E_p = 1.85$ V vs SCE remains irreversible, even when lowering the temperature (Figure 4d), or increasing the scan rate up to 2 V s^{-1} (data not shown). An intermediate case is observed for **5**, for which the second anodic process detected at $E_p = 1.85$ V vs SCE is slightly reversible at −20 °C.

Solvated Complexes 3 and 4. The low oxidation potential of the BPh_4^- anions ($E = 0.9$ V vs SCE) precludes the observation of the anodic Mn(II)/Mn(III) process for complexes $[(L_5^2)Mn(OH_2)](BPh_4)_2$ (**3**$(BPh_4)_2$) or $[(L_5^3)Mn(OH_2)](BPh_4)_2$ (**4**$(BPh_4)_2$). It is however possible to obtain the value of the oxidation potential of cation **3** (**4**) in MeCN solution, by the in situ substitution of the chloride anion of cations $[(L_5^2)MnCl]^+$ (**1**) ($[(L_5^3)MnCl]^+$ (**2**)) by a solvent molecule (either water or MeCN) using silver perchlorate (Figure 4, dashed line) or by mixing stoichiometric quantity of the ligand and of $[Mn(H_2O)_6](ClO_4)_2$. Note that the X-band EPR spectrum of a MeCN solution of the in situ generated complexes **3** and **4** was recorded and compared to the one of a MeCN solution of complexes **3**$(BPh_4)_2$ and **4**$(BPh_4)_2$ and that the two spectra were identical. Addition of 1 equiv. of silver perchlorate per Mn ion to the original solution of **1** (**2**) results in the disappearance of the first anodic wave (peaks 1 and 1′) and the concomitant appearance of the irreversible peak (3) near 1.4 V vs SCE (panels a and c in Figure 4, dotted line). The oxidation process (3) is attributed to the oxidation of the in situ generated species **3** (**4**).

The potential values of the Mn(II)/Mn(III) irreversible oxidation process for the in situ generated complexes **3** and

(67) We have assumed that the Mn—Cl bond length is not significantly shortened in solution compared to the X-ray data.

(68) An approximately $r^{-2.5}$ dependence of Mn(II) zero-field interaction on ligand-metal distance has been proposed by Tabares et al.: Tabares, L. C.; Cortez, N; Agalidis, I.; Un, S. *J. Am. Chem. Soc.* **2005**, *127*, 6039–6047.

(69) Difference in the temperature do not significantly change the pattern of the EPR spectra. Compare, for instance, the spectrum in Figure 3a with that in Figure S1a in the Supporting Information.

(70) Raffard-Pons Y Moll, N.; Banse, F.; Miki, K.; Nierlich, M.; Girerd, J.-J. *Eur. J. Inorg. Chem.* **2002**, 1941–1944.

(71) Balland, V.; Anxolabéhère-Mallart, E.; Banse, F.; Rivière, E.; Bourcier, S.; Nierlich, M.; Girerd, J.-J. *Eur. J. Inorg. Chem.* **2004**, 1225–1233.

(72) Hubin, T. J.; McCormick, J. M.; Collison, S. R.; Buchalova, M.; Perkins, C. M.; Alcock, N. W.; Kahol, P. K.; Raghunathan, A.; Busch, D. H. *J. Am. Chem. Soc.* **2000**, *122*, 2512–2522.

(73) Sabater, L.; Hureau, C.; Blain, G.; Guillot, R.; Thuéry, P.; Rivière, E.; Aukauloo, A. *Eur. J. Inorg. Chem.* **2006**, 4324–4337.

(74) Rogez, G.; Marvilliers, A.; Sarr, P.; Parsons, S.; Teat, S. J.; Ricard, L.; Mallah, T. *J. Chem. Soc., Chem. Commun.* **2002**, 1460–1461.

(75) Rogez, G. *Thesis*, Université Paris-Sud, Orsay, France, 2002.

(76) Neves, A.; Erthal, S. M. D.; Vencato, I.; Ceccato, A. S.; Mascarenhas, Y. P.; Nascimento, O. R.; Hörner, M.; Batista, A. A. *Inorg. Chem.* **1992**, *31*, 4749–4755.

(77) Lanznaster, M.; Neves, A.; Bortoluzzi, A. J.; Assumpção, A. M. C.; Vencato, I.; Machado, S. P.; Drechsel, S. M. *Inorg. Chem.* **2006**, *45*, 1005–1011.

(78) Bernal, I.; Jensen, I. M.; Jensen, K. B.; McKenzie, C. J.; Toftlund, H.; Tuchages, J.-P. *J. Chem. Soc., Dalton Trans.* **1995**, 3667–3675.

(79) Balland, V.; Banse, F.; Anxolabéhère-Mallart, E.; Ghiladi, M.; Mattioli, T. A.; Philouze, C.; Blondin, G.; Girerd, J.-J. *Inorg. Chem.* **2003**, *42*, 2470–2477.

(80) Arulsamy, N.; Glerup, J.; Hodgson, D. J. *Inorg. Chem.* **1994**, *33*, 3043–3050.

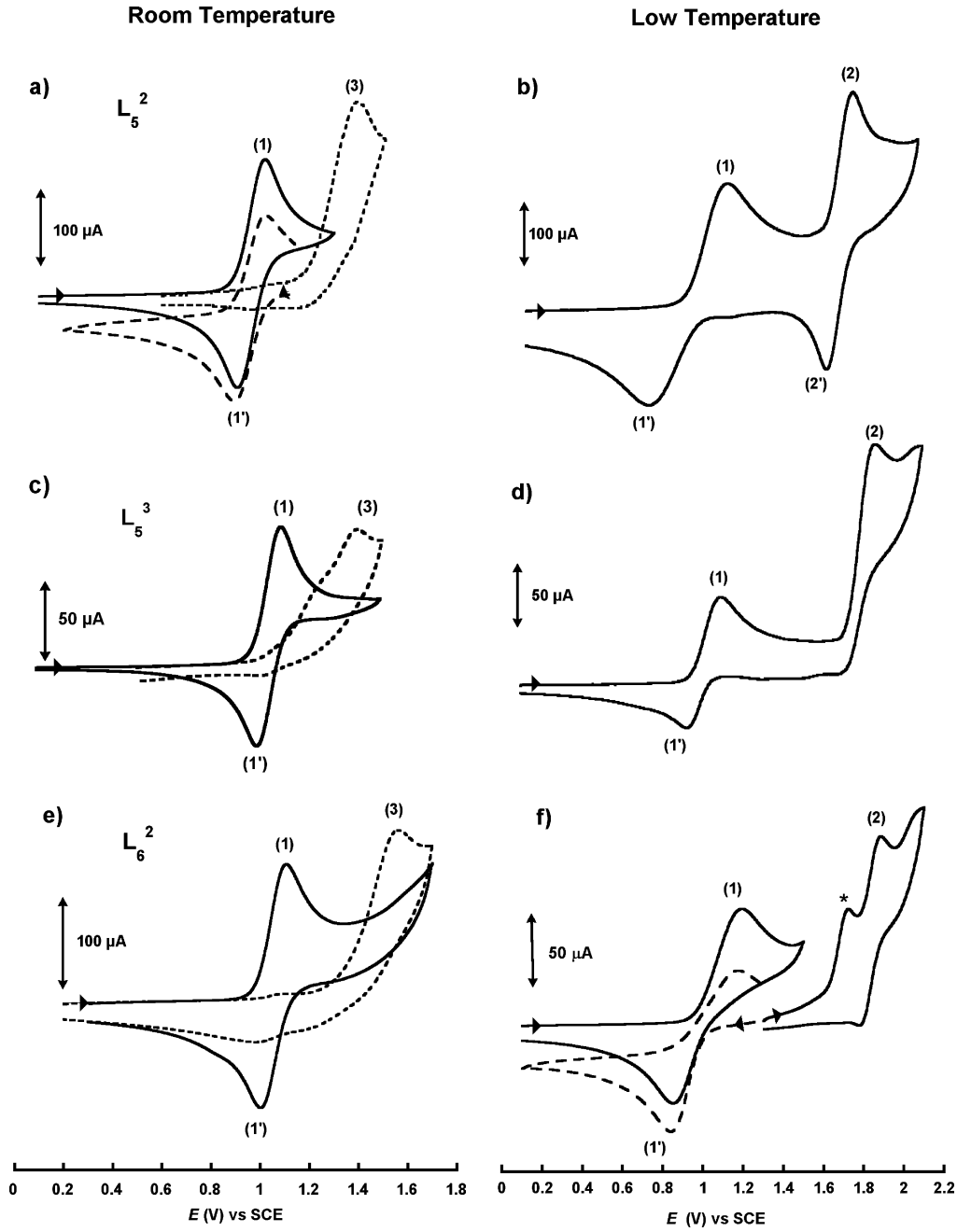

Figure 4. Top: Cyclic voltammetry traces of a 10 mM solution of $[(L_5^2)MnCl]^+$ (**1**) (solid line), after bulk electrolysis at 1.2 V vs SCE (dashed line), and $[(L_5^2)Mn(solvent)]^{2+}$ (**3**) (dotted line) in MeCN containing 0.2 M tetrabutylammonium perchlorate, scan rate = 100 mV/s; (a) $T = 20$ °C and (b) $T = 0$ °C. Middle: Cyclic voltammetry traces of a 5 mM solution of $[(L_5^3)MnCl]^+$ (**2**) (solid line) and $[(L_5^3)Mn(solvent)]^{2+}$ (**4**) (dotted line) in MeCN containing 0.2 M tetrabutylammonium perchlorate, scan rate = 100 mV/s; (c) $T = 20$ °C and (d) $T = -30$ °C. Bottom: Cyclic voltammetry traces of a 10 mM solution of $[(L_6^2)MnCl]^+$ (**5**) (solid line), and of $[(L_5^2)Mn(solvent)]^{2+}$ (**6**) (dotted line); (e) $T = 20$ °C and (f) $T = -20$ °C. Cyclic voltammetry traces of a 10 mM solution of $[(L_6^2)MnCl]^+$ (**5**) after bulk electrolysis at $E = 1.25$ V vs SCE, scanning toward cathodic potentials (dashed line in f) and scanning toward anodic potentials (solid line in f), in MeCN containing 0.2 M tetrabutylammonium perchlorate, scan rate = 100 mV/s. (*) indicates a signal that may be attributed to oxidation process associated to residual amount of **6**.

4 are close to those reported for the related Mn(II) complexes obtained with tetra- or hexadentate amino-pyridine ligand (see Table 6).

The irreversibility of this oxidation process was proposed to arise from the deprotonation of a water molecule bound to the Mn(III) ion. Furthermore, the peak at 1.4 V vs SCE is shifted to 1.3 V vs SCE upon the addition of two equivalents of base (2,6-dimethylpyridine) to the solution. Such a behavior, characteristic of an EC mechanism,[83] was also reported previously for related complexes[55] and is due to an assisted deprotonation of the water molecule in the

(81) Vance, C. K.; Miller, A.-F. *Biochemistry* **2001**, *40*, 13079–13087.
(82) Bard, A. J.; Faulkner, L. R., *Electrochemical Methods, Fundamentals and Applications*; John Wiley and Sons: New York, 2001.
(83) EC stand for electrochemical−chemical and describes a mechanism where the product of the first redox event evolves chemically. See for instance: ref 82.

Table 5. Redox Potentials (V vs SCE) of Mn(II) Complexes Described Here or in Previous Reports and of Isostructural Fe(II) Complexes[a]

	M^{II}/M^{III}			M^{III}/M^{IV}	
complexes	M=Mn	M=Fe	ΔE(Mn/Fe) (mV)	M=Mn	coordination sphere
$[(L_4^2)MCl_2]$	0.740[55]	0.180[70]	560	1.460[55]	N_4Cl_2
$[(L_4^3)MCl_2]$	0.810[55,b]	0.280[70]	530	1.65[55] (irr) [c]	N_4Cl_2
$[(L_6^34Me)M_2Cl_4]$[d,e]	1.100[71]	0.580[71]	520	1.65[71] (irr) [c]	N_3Cl_2
$[(12aneN4)MCl_2]$ [d]	0.466[72]	0.036[72]	430	1.232[72]	N_4Cl_2
$[(14aneN4)MCl_2]$ [d]	0.585[72]	0.110[72]	475	1.343[72]	N_4Cl_2
[(L)MCl] [d]	0.210[73]	−0.140[74,75] [f]	350	1.150[73]	N_4OCl
[(bbpen)M] [d]	−0.06[76,f]	−0.53[77,g]	470	0.80[76,g]	N_4O_2
$[(L_5^2)MCl]^+$	0.950 (this work)	0.570[78]	380	1.65 (this work)	N_5Cl
$[(L_5^3)MCl]^+$	1.020 (this work)	0.640[79]	380	1.85 (this work) (irr) [c]	N_5Cl
$[(L_6^2)MCl]^+$	1.050 (this work)			1.85 (this work) (irr) [c]	N_6Cl
$[(PY5)MCl]^+$ [c]	0.970[43f]	0.710[43,f]	260		N_5Cl
$[(PY5)M(OH)]^+$ [c]	0.600[30]	0.345[31]	255		N_5O
$[(BPTETA)M]^{2+}$ [c]	1.100[31,80]	0.750[80]	350		N_6
$[(4'\text{-X-terpy})_2\ M]^{2+}$[h]	0.78−1.44[32]	0.64−1.15[32]	140−290		N_6
$[(TMG)M(MeCN)]^{2+}$[d]	0.880[46]	0.520[46]	360		N_5
M(Mn)SOD [i,k]	0.050[81]	−0.480[81]	530		N_3O_2
M(Fe)SOD [j,k]	>0.660[81]	−0.020[81]	>680		N_3O_2

[a] The potential values of all complexes were determined in MeCN solvent except for the $[(PY5)Fe(OH)]^+$ complex and the Mn(Fe)SOD, which were determined in DMSO solution and in 100 mM phosphate buffer (pH 7.8), respectively. [b] The $[(L_4^3)MnCl_2]$ complex is obtained in solution by the in situ addition of 1 equiv. per Mn ion of chloride ion on a $[(L_4^3)MnCl(OH_2)]^+$ solution (see ref 55 for details). [c] irr = no cathodic peak was observed on the reverse scan. [d] L_6^34Me = *N*,*N*,*N*′,*N*′-tetrakis[(6-methyl-pyridyl)methyl]-propane-1,3-diamine; 12aneN4 = 4,10-dimethyl-1,4,7,10-tetraazabicyclo[5.5.2]tetradecane; 14aneN4 = 4,11-dimethyl-1,4,8,11-tetraazabicyclo[6.6.2]hexadecane; *L* = *N*,*N*-bis(2-pyridylmethyl)-*N*′-salicylidene-ethane-1,2-diamine; H_2bbpen = *N*,*N*′-bis(2-hydroxybenzyl)-*N*,*N*′-bis(2-pyridylmethyl)-ethane-1,2-diamine; PY5 = 2,6-bis(bis(2-pyridyl)methoxymethane)pyridine; BPTETA = 1,10-bis(2-pyridylmethyl)-1,4,7,10-tetraazadecane; TMG = 1,1,1-tris{2-[N^2(1,1,3,3-tetramethylguanidino)]ethyl}amine. [e] The dimeric Mn or Fe complexes can be considered as two mononuclear Mn or Fe species with a N_3Cl_2 coordination sphere separated by a propylene bridge. [f] The given value corresponds to the one reported in ref 75, for which the reversible electrochemical process was observed in the presence of 3 equiv. of chloride ion. [g] The value of $E(Fc/Fc^+)$ = 0.307 vs SCE[82] was used to convert the original data. [h] $[(4'\text{-X-terpy})_2M]^{2+}$ corresponds to Mn or Fe complexes containing a series of 4′-substituted 2,2′:6′,2″-terpyridine (terpy) ligands. The substituent X was (in order of electrowithdrawing effect) −Cl, −H, $-CH_3Ph$, −OH, or −pyrrolidine. We report here only the two extreme values, i.e., for −Cl and −pyrrolidine substituted ligands. [i] MnSOD from *E. coli* with the native metal (M = Mn) or substituted by Fe (M = Fe). [j] FeSOD from *E. coli* with the native metal (M = Fe) or substituted by Mn (M = Mn). [k] SCE = 0.24 V vs NHE.

Table 6. Peak Potentials (V vs SCE) of Mn(II) Complexes Described Here or in Previous Reports[a]

complexes	E_p
$[(L_4^2)Mn(solvent)_2]^{2+}$[b,c]	1.3[55]
$[(L_4^3)Mn(solvent)_2]^{2+}$ [b,c]	1.4[55]
$[(L_5^2)Mn(solvent)]^{2+}$[b,c] (**3**)	1.4 (this work)
$[(L_5^3)Mn(solvent)]^{2+}$[b,c] (**4**)	1.4 (this work)
$[(L_6^2)Mn(solvent)]^{2+}$ [b,c] (**6**)	1.5 (ref 34 and this work)

[a] The potential values of all complexes were determined in MeCN solvent. [b] In situ generated complexes by precipitation of the adequate number of chloride ligands. [c] Solvent = MeCN or water.

presence of base. This supports the generation, at least intermediately, of the aqua complex $[(L_5^2)Mn(OH_2)]^{3+}$ upon oxidation of species **3**.

Bulk Electrolyses of Chloro Species 1, 2, and 5. Evolution of the Electrochemically Generated Mn(III) Complexes. From the cyclic voltammetry, it is anticipated that the Mn(III) $[(L_5^2)MnCl]^{2+}$, $[(L_5^3)MnCl]^{2+}$ and $[(L_6^2)MnCl]^{2+}$ complexes could be obtained from the corresponding Mn(II) $[(L_5^2)MnCl]^+$ (**1**), $[(L_5^3)MnCl]^+$ (**2**) and $[(L_6^2)MnCl]^+$ (**5**) complexes. The following part describes the electrochemical generation of the $[(L_5^2)Mn(III)Cl]^{2+}$ (**7**) and $[(L_6^2)Mn(III)Cl]^{2+}$ (**8**) complexes by preparative scale electrolyses. The generation of the Mn(III) species is followed by UV−vis absorption and X-band EPR spectroscopies. The bulk electrolyses of the 10 mM solution of **1** and **5** were performed at 1.2 V vs SCE and the measured charge quantity indicated a 1 e^-/Mn process. Cyclic voltammetry traces recorded on the electrolyzed solutions (Figure 4a, dashed line and Figure 4f, dashed line, respectively) confirm that **7** and **8** have been quantitatively generated. It has to be noted that performing the electrolysis of **5** at 20 °C precludes the detection of the cathodic wave at $E_{1/2}$ = 1.05 V vs SCE indicating a more complex behavior when the temperature is not lowered.

During the course of the electrolyses of **1** and **5**, the colorless solutions turned pink. The evolution of the UV−vis absorption spectra are presented in Figure 5 and the UV−vis data calculated on the basis of a 100% oxidation of the initial Mn(II) complex into Mn(III) are gathered in Table 7 together with those of the related $[(L_4^2)Mn(III)Cl_2]^+$ complex.[55] The low energy λ_2 and λ_3 bands are attributed to Mn(III) d−d transitions in agreement with the low extinction coefficients theoretically expected for such transitions.[84] Those bands appear at higher energy in **7** than in the case of $[(L_4^2)Mn(III)Cl_2]^+$. This is related to the substitution of the chloride ion presenting a weak ligand field by a pyridine ligand having a higher field strength. Again, a slight bathochromic effect is observed between **7** and **8** because of the presence of an additional pyridine group in the latter complex. The higher energy band at λ_1 is attributed to a Cl^- to Mn(III) charge transfer[85,86] and is less intense (by a factor close to 2) in the monochloro complexes **7** and **8** than the one observed in the case of the dichloro complex $[(L_4^2)Mn(III)Cl_2]^+$.

The evolution of the X-band EPR spectra recorded in the conventional perpendicular detection mode and in parallel mode shows the progressive disappearance of the signatures of **1** and **5** (see Figures S1 and S2 in the Supporting Information, respectively). The lack of signal in the EPR spectrum recorded using the perpendicular detection mode

(84) Dingle, R. *Acta Chem. Scand.* **1966**, *20*, 33–44.
(85) Goodwin, H. A.; Sylva, R. N. *Aust. J. Chem.* **1965**, *18*, 1743–1749.
(86) Sarneski, J. E.; Thorp, H. H.; Brudvig, G. W.; Crabtree, R. H.; Schulte, G. K. *J. Am. Chem. Soc.* **1990**, *112*, 7255–7260.

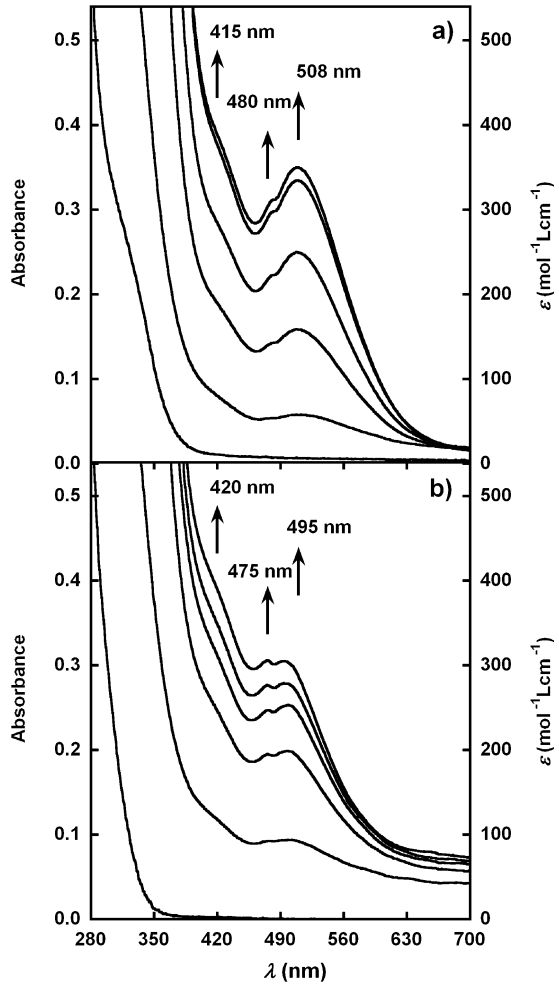

Figure 5. Evolution of the UV−vis spectrum of a 10 mM MeCN solution (a) of $[(L_5^2)MnCl]^+$ (**1**), upon preparative scale electrolysis at $E = 1.2$ V vs SCE, $T = 20$ °C, $l = 1$ mm; and (b) $[(L_6^2)MnCl]^+$ (**5**) upon preparative scale electrolysis at $E = 1.1$ V vs SCE, $T = -20$ °C, $\mathbf{l} = 1$ mm.

on the electrolyzed solutions after the completion of the 1e⁻/Mn oxidation agrees with the +III oxidation state of the Mn oxidized species. A signal was detected at $g_{eff} = 8.9$ (**7**) and $g_{eff} = 9.0$ (**8**) on the 9.4 GHz EPR spectra recorded using the parallel detection mode (see Figure S2 in the Supporting Information). As previously described in the literature, X-band parallel detection mode spectra are expected for nearly axial $S = 2$ systems with strong Zero-Field Splitting.[87,88] Unfortunately, no hyperfine lines were detected unlike what has been previously described in the case of $[(L_4^2)Mn(III)Cl_2]^+$.[55]

The reversibility of the Mn(II)/Mn(III) oxidation process relative to cation **2**, observed in the cyclic voltammetry time scale (Figure 4c) suggested the possible formation of the $[(L_5^3)Mn(III)Cl]^+$ cation. However, in the course of the low temperature electrolysis (−30 °C), the initially colorless solution turned first reddish, but immediately evolved to dark brown color. Therefore the mononuclear $[(L_5^3)Mn(III)Cl]^+$ cation is not stable in MeCN solution, on the contrary to what was observed with the formation of cations **7** and **8**.

(87) Hendrich, M. P.; Debrunner, P. G *Biophys. J.* **1989**, *56*, 489–506.
(88) Krzystek, J.; Yeagle, G. J.; Park, J.-H.; Britt, R. D.; Meisel, M. W.; Brunel, L.-C.; Telser, J. *Inorg. Chem.* **2003**, *42*, 4610–4618.

The preliminary spectroscopic and cyclic voltammetry studies suggested the presence of several high-valence species in the oxidized solution. The formation of μ-oxo dinuclear entities as well as species of higher nuclearity is also anticipated, but determination of the exact nature of these species is out of the scope of the present paper.

Electrochemical and Chemical Oxidations of Solvated Species 3 and 4. We have recently reported examples of the electrochemical preparation of mixed-valence di-μ-oxo $[(L)Mn(III)(\mu O)_2Mn(IV)(L)]^{3+}$ dinuclear complexes with tetradentate[55] and hexadentate[34] amino-pyridine ligands from the corresponding solvated Mn(II) species. In the latter case, the $[(L_6^2)Mn(III)(\mu O)_2Mn(IV)(L_6^2)]^{3+}$ (**10**) complex was generated, in which two out of the four pyridine arms of the L_6^2 ligand were decoordinated. Thus, we have investigated here the electrochemical oxidation of the in situ generated cations $[(L_5^2)Mn(OH_2)]^{2+}$ (**3**) and $[(L_5^3)Mn(OH_2)]^{2+}$ (**4**) in presence of an external base. In the case of **3**, the formation of the $[(L_5^2)Mn(III)(\mu O)_2Mn(IV)(L_5^2)]^{3+}$ (**9**) was clearly evidenced by cyclic voltammetry, X-band EPR, and UV−vis absorption spectroscopies (see Figures S7−S9 in the Supporting Information). On the contrary, in the case of complex **4**, the electrochemical preparation led to the formation of a mixture of several μ-oxo bridged polynuclear complexes, the nature of which has not been elucidated yet.

Similarly, the chemical synthesis of the mixed-valence di-μ-oxo complex (**9**) from H_2O_2 oxidation of a Mn(II)/ligand mixture in water is successful (elemental analysis, IR, EPR, and UV−visible spectra as well as the cyclic voltammetry signature are given in Figures S3−S6 in the Supporting Information), whereas the one starting from the L_5^3 ligand was always thwarted. Once again, these observations pinpoint a different behavior in solution between complexes obtained with $L_{5/6}^2$ and L_5^3 ligands that we try to analyze in the next paragraph.

Discussion

The first part of the discussion deals with the behavior's difference encountered upon oxidation for various species made with L^2 or L^3 ligands (L^2 and L^3 ligands are built on the 1,2-diamino-ethane or on the 1,3-diamino-propane spacer, respectively as shown in Chart 1). In a second part, we comment on the redox properties of the series of Mn complexes described in this paper, and in a third part, we analyze the differences in the redox properties of Mn vs Fe isostructural species in the context of what is known for the Mn/Fe SOD system.

Reactivity Difference between L^2 and L^3. The different responses upon oxidation between the chloro cations $[(L_5^2)MnCl]^+$ (**1**) and $[(L_5^3)MnCl]^+$ (**2**), on one hand and between cations $[(L_5^2)Mn(OH_2)]^+$ (**3**) and $[(L_5^3)Mn(OH_2)]^+$ (**4**), on the other, can be better understood with the help of other related examples. Consequently, we gather the published structural data on Mn and Fe mononuclear complexes and on their oxidized dinuclear counterparts in Table 8. We have decided to limit the comparison to complexes with amino-pyridine tetra (L_4) and pentadente (L_5) ligands, the

Table 7. UV−vis Data for Electrochemically Prepared Complexes $[(L_5^2)MnCl]^{2+}$ (**7**) and $[(L_6^2)MnCl]^{2+}$ (**8**); Data on $[(L_4^2)Mn(III)Cl_2]^{+}$[55] Species Are Included for Comparison

	$[(L_4^2)Mn(III)Cl_2]^+$	**7**	**8**	attribution
λ_1 (nm), ε_1 (mol^{-1} L cm^{-1})	394,1150	415, 390	420, 395	Cl^- to Mn(III) LMCT
λ_2 (nm), ε_2 (mol^{-1}L cm^{-1})	500, 300	480, 310	475, 305	d−d transition
λ_3 (nm), ε_3 (mol^{-1} L cm^{-1})	538, 360	508, 350	495, 295	d−d transition

Table 8. Configurations of the Ligands L_4^n and L_5^n in mono- and dinuclear Mn or Fe Complexes[a]

L	Mn				Fe			
	mononuclear Mn(II)		dinuclear Mn(III)Mn(IV)		mononuclear Fe(II)		dinuclear Fe(III)Fe(III)	
L_4^2	$[LMnCl_2]$ [55]	cis-α	$[LMn(\mu O)_2MnL]^{3+}$ [55]	cis-α	$[LFeCl_2]$ [70]	cis-α	$[L(Cl)Fe(\mu O)Fe(Cl)L]^{2+}$[70]	cis-α
L_4^3	$[LMnCl(OH_2)]^+$ [55]	cis-β	$[LMn(\mu O)_2MnL]^{3+}$[55]	cis-α	$[LFeCl_2]$ [70]	cis-α	$[(Cl)_3Fe(\mu O)Fe(Cl)L]$ [70]	cis-β
			$\{[L(Cl)Mn(\mu O)Mn(Cl)L]^{3+}\}$ [55]	cis-β				
L_5^2	$[LMnCl]^+$ (**1**)	mer−cis	$\{[LMn(\mu O)_2MnL]^{3+}\}$ (this work)	cis-α	$[LFeCl]^+$ [89]	mer−cis	$[L(Cl)Fe(\mu O)Fe(Cl)L]^{2+}$ [90]	cis-α
	$[LMn(OH_2)]^{2+}$ (**3′**)	mer−cis						
	$[LMn(OH_2)]^{2+}$ (**3**)	mer−trans						
L_5^3	$[LMnCl]^+$ (**2**)	mer−cis			$[LFeCl]^+$ [79]	mer−cis	$\{[(Cl)_3Fe(\mu O)Fe(Cl)L]\}$ [79]	cis-β
	$[LMn(OH_2)]^{2+}$ (**4**)	mer−trans						

[a] Complexes for which the proposed structure relies on spectroscopic studies are bracketed. Other complexes have been X-ray characterized.

latter ligand being obtained by substitution of one methyl group by a pyridine in the L_4ligands (see Chart 1).

For hexacoordinated metal ions, the linear tetradente L_4 ligand can adopt three configurations: the cis-α and the cis-β drawn in Scheme 1 and the trans configuration obtained when the two exogenous ligand are in trans position while the four nitrogen atoms of the linear tetradentate ligand are planar. This latter configuration has not been observed until now. The pentadentate ligand L_5 can also adopt three configurations: the mer−cis and mer−trans drawn in Scheme 1 and the fac configuration obtained when the three pyridine groups are in a facial arrangement, this latter one being not observed yet. It is worth noting that the minimal rearrangement that allows switching from a L_5 ligand to the corresponding L_4 linear ligand is the decoordination of one pyridine group.[91] In case of a mer−cis configuration of the L_5 ligand, this leads to either the cis-α or cis-β configurations, whereas in case of a mer−trans configuration, this leads only to the cis-β configuration. (see Scheme 1).

From the data reported in Table 8, it appears that the L_4^2 ligand can only adopt the cis-α configuration in contrast to the L_4^3 ligand that can fit both to the cis-α and cis-β configurations. The former is observed in dinuclear Mn complexes and in mononuclear Fe species while the latter is encountered in both mono- and dinuclear Mn complexes and only in dinuclear Fe species. Concerning the L_5 ligand, the two mer−cis and mer−trans configurations are encountered in Mn mononuclear cations, both configuration being observed for the $[(L_5^2)Mn(OH_2)]^+$ species in **3** and **3′**. This may be related to the difference in the counterion present in the crystal structure of **3** (BPh_4^-) and **3′** (ClO_4^-). Similar counterion effect has been encountered in the case of the $[(bpa)_2M]^{2+}$ complexes, where bpa is the tridentate amino-pyridine bis(2-pyridylmethyl)amine ligand. In case of the $[(bpa)_2M]Cl_2$ (M = Fe,[92] Co,[92] Zn,[93] Ni[94]) complexes, the bpa ligand is in a facial configuration with the two amine functions in trans position, whereas in the case of the $[(bpa)_2M](ClO_4)_2$ (M = Fe,[95] Cu,[96] Mn, [93] Ni, [97] Hg[98]) the two amine functions are in a cis position with bpa in facial configuration. In other words, presence of the Cl^- (ClO_4^-) is related to the trans (cis) of the amine functions. We conjecture that different interactions (hydrogen bonds, stacking, etc.) between the complex and the counterion are responsible for the different configurations observed between **3** and **3′** as well as in the case of $[(bpa)_2M]^{2+}$ complexes. Only the mer−cis configuration is detected in case of Fe, an observation that can tentatively be attributed to the difficulty to isolate the Fe aqua species.

The nature of the complexes resulting from the decoordination of one pyridine[91] and dimerization are best explained if we make the hypothesis that (i) the L_5^2 (L_5^3) ligand switches to a cis-α (cis-β) configuration; (ii) a cis-α configuration is associated to the isolation of a $[Mn(\mu O)_2Mn]^{3+}$ and a $[(Cl)Fe(\mu O)Fe(Cl)]^{2+}$ cores, whereas a cis-β configuration is related to the formation of a $[(Cl)Mn(\mu O)Mn(Cl)]^{3+}$ core and a $[(Cl_3)Fe(\mu O)Fe(Cl)]$ asymmetric core.

However, these structural aspects are not sufficient to explain all the differences observed between complexes obtained with L^2 or L^3 ligands upon oxidation. For instance, cations **1** and **2** are both in mer−cis configuration but

(89) Mialane, P.; Nivorojkine, A.; Pratviel, G.; Azéma, L.; Slany, M.; Godde, F.; Simaan, A.; Banse, F.; Kargar-Grisel, T.; Bouchoux, G.; Sainton, J.; Horner, O.; Guilhem, J.; Tchertanova, L.; Meunier, B.; Girerd, J.-J. *Inorg. Chem.* **1999**, *38*, 1085–1092.

(90) Nivorozhkin, A. L.; Anxolabéhère-Mallart, E.; Mialane, P.; Davidov, R. Y.; Guilhem, J.; Cesario, M.; Audière, J.-P.; Girerd, J.-J.; Styring, S.; Schussler, L.; Seris, J.-L. *Inorg. Chem.* **1997**, *36*, 846–853.

(91) The decoordinated pyridine group are held by the amine function bearing the two pyridine functions, else the tetradentate ligand obtained is tripodal not linear.

(92) Davies, C. J.; Solan, G. A.; Fawcett, J. *Polyhedron* **2004**, *23*, 3105–3114.

(93) Glerup, J.; Goodson, P. A.; Hodgson, D. J.; Michelsen, K.; Nielsen, K. M.; Weihe, H. *Inorg. Chem.* **1992**, *31*, 4611–4616.

(94) Fleury, B.; Mallah, T. 2008, personal communication.

(95) Liu, C.-M.; Gao, H.-Y.; Zhang, D.-Q.; Zhu, D.-B. *Lett. Org. Chem.* **2005**, *2*, 712–715.

(96) Huang, G.-S.; Lai, J.-K.; Ueng, C.-H.; Su, C.-C. *Transition Met. Chem.* **2000**, *25*, 84–92.

(97) Velusamy, M.; Palaniandavar, M.; Thomas, K. R. J. *Polyhedron* **1998**, *17*, 2179–2186.

(98) Bebout, D. C.; DeLanoy, A. E.; Ehmann, D. E.; Kastner, M. E.; Parrish, D. A.; Butcher, R. J. *Inorg. Chem.* **1998**, *37*, 2952–2959.

oxidation to the corresponding Mn(III) is only possible in case of **1**. Similarly, formation of di-μ-oxo bridge binuclear complex can be achieved in case of **3** and was always unsuccessful in case of **4**. Consequently, the increased flexibility of the 6- vs the 5-membered metallacycle is not only responsible for a different configuration accommodation but also for other factors that contribute to the distinct reactivity.

An interesting point that should also be mentioned is that reactivity of the Fe dinuclear complexes upon alkane hydroxylation is enhanced with the asymmetric core [(Cl_3)Fe(μO)Fe(Cl)] complexes obtained in the case of $L_4{}^3$[70,99] and $L_5{}^3$[99] and that similar results in alkene epoxidations have been described with Mn complexes obtained with $L_6{}^3$ ligand compared to $L_6{}^2$ (see Chart 1).[100]

Lastly, for a given ligand, the diversity in the synthetic routes required to form the dinuclear Mn or Fe complexes (see references in Table 8) as well as the difference in the dinuclear Mn and Fe cores obtained suggest a distinct behavior of the two metallic ions upon condensation. We propose that one possible explanation is the difference in the redox potentials of the Mn(II) or Fe(II) mononuclear entities. We will comment on the origins of such differences in the last part of the discussion.

Redox Properties of Mn(II) Complexes. Table 5 gathers the $E_{1/2}$ potential values for complexes **1**, **2**, and **5** together with values of the [$(L_4{}^2)MnCl_2$] and [$(L_4{}^3)MnCl_2$] complexes as well as those of the corresponding mononuclear Fe complexes, except for the heptacoordinated species **5** that has not its Fe analogue (see Chart 1 for the nomenclature of the ligands). The charge of the complexes is the predominant factor that influence the $E_{1/2}$ potential value, with a difference of 210 mV observed between the neutral complexes [$(L_4{}^2)MnCl_2$] ([$(L_4{}^3)MnCl_2$]) and the monocationic complexes **1** (**2**). The $E_{1/2}$ values reported for complexes **1**, **2**, and **5** for the Mn(II)/Mn(III) redox process are within the range of the one reported for Mn(II) complexes with [N_5Cl] coordination sphere[39,43] or slightly higher than those with topologically constrained [N_5Cl][40] or [N_4Cl][72] coordination sphere. A 70 mV (100 mV) potential difference between the Mn(II)/Mn(III) redox couples of **1** (ligand $L_5{}^2$) and **2** (ligand $L_5{}^3$) (**1** (ligand $L_5{}^2$) and **5** (ligand $L_6{}^2$)) is observed. In other words, the $E_{1/2}$ potential will be moved toward positive values for the bulkier complexes **2** and **5** compared to **1**. Similar shifts of the potential value have been already reported in the case of other Mn complexes[55,101] and of related Fe complexes.[71,99,102] A maximum increase of about ~120 mV has been reported by Hubin for the $E_{1/2}$ potential value of the Mn(II)/Mn(III) oxidation process when increasing the size of the cross-bridged tetraazamacrocycles ligand from 12-membered ring to 14-membered.[72] These potential shifts can be related to the difference in the solvatation energy gained in the course of the Mn(II) to Mn(III) oxidation process. The smaller the radius of the equivalent sphere of the Mn complex is,[103] the more important the stabilization energy due to the solvent.[104] In addition, it is noteworthy that the 70 mV potential difference between the M(II)/M(III) redox couples of complexes [$(L_5{}^2)MCl]^+$ and [$(L_5{}^3)MCl]^+$ (M = Mn, Fe) are very close to the one measured for complexes [$(L_4{}^2)MCl_2$] and [$(L_4{}^3)MCl_2$] (M = Mn, Fe). As a consequence, in term of potential, the effect of one additional carbon on the alkyl chain (propyl vs ethyl spacer) is independent of the metal center and of the denticity of the ligand and can thus be viewed as a second coordination sphere effect.

Comparison of the M(II)/M(III) Redox Potential for M = Mn and Fe. In the previous part, we have commented on the redox potential values of the Mn(II) complexes described in this paper with the help of complexes with closely related coordination sphere. In this part, we examine the factors that influence the difference between the redox potentials values of Mn(II) and Fe(II) analogous complexes, in other words how the coordination sphere affects the redox properties of Mn(II) compared to that of Fe(II).

In addition to the Mn complexes investigated in the present work, we have gathered in Table 5 the M(II)/M(III) $E_{1/2}$ potential values for a series of Mn and Fe complexes from the literature together with the one reported for MnSOD and FeSOD. We deliberately limit the comparison to complexes obtained with nonporphyrinic ligand and with a [N,O,Cl^-] coordination sphere. Because we only consider reversible redox processes, the data reported do not include complexes with bound water molecules. Indeed, as we exemplified with species [$(L_5{}^2)Mn(OH_2)]^+$ (**3**) and [$(L_5{}^3)Mn(OH_2)]^+$ (**4**), the presence of labile solvent ligand that can be exchanged by a water ligand leads to the irreversibility of the oxidation process. As commonly experienced, the redox potentials (M(II)/M(III)) of Mn complexes are higher than those of the structurally analogous Fe complexes. Such an effect can be related to the filling of the d-orbitals. Indeed, oxidation of Fe(II) complexes is easier because it leads to a half-filled shell while oxidation of Mn(II) species induces the loss of the half-filled shell. With the objective of better understanding the parameters that differentiate the Mn and Fe complexes from a redox point of view, we plot a representation of the potential difference between Mn(II)/Mn(III) and Fe(II)/Fe(III) couples (ΔE(Mn/Fe)) as a function of the charge of the complex in the reduced state (see Figure 6).

We first observed that ΔE(Mn/Fe) tends to decrease with the increase of the formal charge of the complex. For example ΔE(Mn/Fe) is smaller in the case of the monocationic complexes [$(L_5{}^2)MCl]^+$ and [$(L_5{}^3)MCl]^+$ (380 mV) than in the case of the related neutral [$(L_4{}^2)MCl_2$] and

(99) Raffard, N.; Balland, V.; Simaan, J.; Létard, S.; Nierlich, M.; Miki, K.; Banse, F.; Anxolabéhère-Mallart, E.; Girerd, J.-J. C. R. *Chimie* **2002**, *5*, 99–109.
(100) Brinksma, J.; Hage, R.; Kerschner, J.; Feringa, B. L. *J. Chem. Soc., Chem. Commun.* **2000**, 537–538.
(101) Gultneh, Y.; Yisgedu, T. B.; Tesema, Y. T.; Butcher, R. J. *Inorg. Chem.* **2003**, *42*, 1857–1867.
(102) Simaan, J.; Poussereau, S.; Blondin, G.; Girerd, J.-J.; Defaye, D.; Philouze, C.; Guilhem, J.; Tchertanov, L. *Inorg. Chim. Acta* **2000**, *299*, 221–230.
(103) According to the Born model theory, a sphere of radius r_i and charge $z_i e_0$ is considered to be equivalent to an ion of radius r_i and charge $z_i e_0$. In the present case, we consider the Born model theory to evaluate the variation of solvatation energy upon Mn(II)/Mn(III) redox process.
(104) Bockris, J. O. M.; Reddy, A. K. N., *Modern Electrochemistry*; Plenum: New York, 1973; Vol. *1*, Chapter 2.

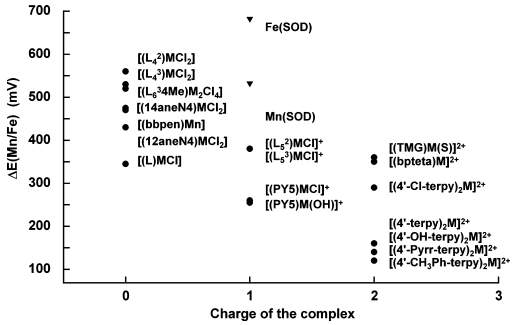

Figure 6. Variation of the potential difference between Mn(II)/Mn(III) and Fe(II)/Fe(III) couples (ΔE(Mn/Fe)) with the global charge of various Mn(II) and Fe(II) systems (see text and ref 105). The complexes are those from Table 5. Note that the value for the Mn(Fe)SOD is a lower value and that data points for complexes $[(L_5^2)MCl]^+$ and $[(L_5^3)MCl]^+$ are overlapped as well as those for complexes $[(4'\text{-OH-terpy})_2M]^{2+}$ and $[(4'\text{-terpy})_2M]^{2+}$.

$[(L_4^3)MCl_2]$ (560−530 mV). A second effect is the effective net charge on the metal center. This has been recently described and discussed with the help of quantum chemical calculations on the series of $[(4'\text{-X-terpy})_2M]^{2+}$ for which the ΔE(Mn/Fe) tend to increase with the enhancement of the electrowithdrawing properties of the X substituent.[32] Third, for a given charge and closely related complexes, the nature of the ligand in the coordination sphere influences the ΔE(Mn/Fe) value. For example, ΔE(Mn/Fe) equals 560 mV for the $[(L_4^2)MCl_2]$ complex and the replacement of the two chloride ions by two phenolate groups leading to the [(bbpen)M] complex results in a decrease of 90 mV of the ΔE(Mn/Fe) value (470 mV). However, complexes [(L)MCl] having a mixed chloride-phenolate coordination sphere show an even smaller value of ΔE(Mn/Fe) (350 mV) than the one of the [(bbpen)M] complex. Such observations preclude any simple rationalization with ligand field theory. This is still more obvious when comparing the $[(PY5)MCl]^+$ and $[(PY5)M(OH)]^+$ systems for which the exogenous chloride having a weak ligand field or hydroxide having a strong ligand field indeed lead to almost identical ΔE(Mn/Fe) values. Such data are intriguing. However a possible explanation is that the rigidity of the PY5 ligand has an important effect on the ΔE(Mn/Fe) values in that case. Contribution of the rigidity of the ligand is indeed the fourth parameter that influence the ΔE(Mn/Fe) value. Such contribution is even more obvious when considering the ΔE(Mn/Fe) difference observed between complexes with coordination sphere of identical atoms donor set but distinct geometrical constrains. Indeed, the ΔE(Mn/Fe) value is lower in complexes $[(12aneN4)MCl_2]$ or $[(14aneN4)MCl_2]$ where the ligands are ultrarigid cross-bridged tetraazamacrocycles[72] compared to complexes $[(L_4^2)MCl_2]$ and $[(L_4^3)MCl_2]$ (450 mV vs 545 mV, in average). The same conclusion can be drawn from the comparison of complex [(PY5)MCl] where the PY5 ligand is a rigid pentadentate clamp that was shown to enforce a distorted-octahedral coordination geometry,[43] with the $[(L_5^{2/3})MCl]$ complex (260 mV vs 380 mV). Interestingly, the five-coordinated $[(L_6^3 4Me)M_2Cl_4]$ have ΔE(Mn/Fe) values similar to those of the related hexacoordinated $[(L_4^2)MCl_2]$ complex. This indicates that it is more likely the rigidity imposed by the ligand than the geometry by itself that is responsible for the differences observed in the ΔE(Mn/Fe) values. Indeed, rigidity due to the ligand can favor one over the other oxidation state thus influencing the redox potential and would have different impact on Mn vs Fe complex. For instance, a Mn complex where the ligand assist the Jahn−Teller distortion of the Mn(III) ion would be easier to oxidize while the oxidation of the analogous Fe complex would not be affected (see ref 53 and references therein for a relevant example). Such an effect of the ligand rigidity can be related to the entatic effect encountered in proteins.

Last but not least, the data obtained for the SOD[105] appear clearly beyond the trend found for synthetic models. We cannot exclude that the different potential determination methods for the SOD and the chemical complexes are at the origin of such discrepancy, but additional parameters must also be considered. We need to mention that the natural donor set of SOD is far from being comparable to the donor sets considered in the present work. In the present comparison only chemically reversible redox processes have been considered for complexes with saturated coordination sphere. Closer modeling of the SOD donor set requires the insertion of a coordinated water molecule. In that last case, we have observed that the redox process became irreversible (see Table 6), thus precluding the determination of a thermodynamically meaningful potential. As a consequence, discrepancy between the chemical models plotted in Figure 6 and the SOD can be related to a possible proton coupled electron transfer in SOD.[106] This last hypothesis is strengthened by the fact that the potential values are clearly different in Fe or MnSOD despite a structurally homologous coordination sphere.

Perspectives. The origin of the variation of the ΔE(Mn/Fe) value is difficult to unravel and the above-mentioned observations illustrate that its fine-tuning is governed by several parameters. The ΔE(Mn/Fe) value can be modulated by playing with either the formal charge of the complex (the more charged the complex, the weaker the ΔE(Mn/Fe) value) or the real charge of the metal center (modification of the ligand with electron withdrawing groups)[32] or by imposing a geometrical constrain.

We can now try to relate these observations to what is observed in Mn(Fe)SOD and Fe(Mn)SOD.[20] Vance and coworkers proposed that the apparent inactivity of such substituted SOD reflects either lower (Fe(Mn)SOD) or higher (Mn(Fe)SOD) redox potentials than those of the native Fe or MnSOD.[13,81] In contrast the so-called cambialistic SOD maintain their activity upon metal substitution. Yikilmaz and co-workers have proposed a hydrogen-bond interaction to be at the origin of the fine redox tuning of the metal and have provided experimental support that the protein matrix can apply significant redox tuning via its influence over redox-coupled proton transfer.[106] The role of the coordinated solvent ligand has also been noted with regards to redox tuning of the active site.[21,22] The present work supports the

(105) Charge of the active site of SOD from ref 14.
(106) Yikilmaz, E.; Xie, J.; Brunold, T. C.; Miller, A.-F. *J. Am. Chem. Soc.* **2002**, *124*, 3482–3483.

idea that has been previously reported[21,22] that more distant contribution than the primary ligand sphere may be at the origin of the metal-specific activity and suggests that this proton-coupled electron transfer predominate over the effects encountered in chemical models in the present study. As a direct consequence, the preparation of cambialistic SOD models will require the design of mononuclear Mn/Fe complexes with bound water molecule. The ligand should thus be a sterically encumbered scaffold designed to wrap around the metal center leaving a labile site for the coordination of the water molecule. Further sophistication will involve regulation of the secondary coordination sphere of the metal center by appending a series of potential proton acceptors mimicking the H-bond interaction described in SOD.

Acknowledgment. We thank the Conseil Général d'Ile de France for financial contribution in support of the Bruker ELEXSYS 500 X-band EPR spectrometer. S.G. thanks the LCR-CEA project for financial support.

Supporting Information Available: Electrochemical oxidations of $[(L_5^2)MnCl]^+$ (**1**) into $[(L_5^2)MnCl]^{2+}$ (**7**) and of $[(L_6^2)MnCl]^+$ (**5**) into $[(L_6^2)MnCl]^{2+}$ (**8**) including perpendicular and parallel modes X-band EPR spectra (Figures S1 and S2); synthesis of $[(L_5^2)Mn(\mu O)_2Mn(L_5^2)](ClO_4)_3 \cdot 3H_2O$ (**9**$(ClO_4)_3 \cdot 3H_2O$) with complete characterizations: Figure S3, ESI -MS; Figure S4, solid state IR; Figure S5, solution X-band EPR; and Figure S6, cyclic voltammetry); UV−vis (Figure S7), EPR (Figure S8), and cyclic voltammetry (Figure S9) monitoring of the electrochemical conversion of **1** into $[(L_5^2)Mn(\mu O)_2Mn(L_5^2)]^{3+}$ (**9**) (PDF); Crystallographic information in CIF format. This material is available free of charge via the Internet at http://pubs.acs.org.

IC8015172